© 2019. Published by The Company of Biologists Ltd | Journal of Cell Science (2019) 132, jcs228023. doi:10.1242/jcs.228023

RESEARCH ARTICLE

WIP-1 and DBN-1 promote scission of endocytic vesicles by bridging actin and Dynamin-1 in the *C. elegans* intestine

Xuemeng Shi[1,§], Fengyun Duan[1,§,*], Long Lin[1,‡], Qifeng Xu[1], Tao Xu[1,2,¶] and Rongying Zhang[1,¶]

ABSTRACT

There has been a consensus that actin plays an important role in scission of the clathrin-coated pits (CCPs) together with large GTPases of the dynamin family in metazoan cells. However, the recruitment, regulation and functional interdependence of actin and dynamin during this process remain inadequately understood. Here, based on small-scale screening and *in vivo* live-imaging techniques, we identified a novel set of molecules underlying CCP scission in the multicellular organism *Caenorhabditis elegans*. We found that loss of Wiskott–Aldrich syndrome protein (WASP)-interacting protein (WIP-1) impaired CCP scission in a manner that is independent of the *C. elegans* homolog of WASP/N-WASP (WSP-1) and is mediated by direct binding to G-actin. Moreover, the cortactin-binding domain of WIP-1 serves as the binding interface for DBN-1 (also known in other organisms as Abp1), another actin-binding protein. We demonstrate that the interaction between DBN-1 and F-actin is essential for Dynamin-1 (DYN-1) recruitment at endocytic sites. In addition, the recycling regulator RME-1, a homolog of mammalian Eps15 homology (EH) domain-containing proteins, is increasingly recruited at the arrested endocytic intermediates induced by F-actin loss or DYN-1 inactivation, which further stabilizes the tubular endocytic intermediates. Our study provides new insights into the molecular network underlying F-actin participation in the scission of CCPs.

This article has an associated First Person interview with the first author of the paper.

KEY WORDS: Clathrin-coated vesicles, Scission, Actin, WIP-1, DBN-1, *Caenorhabditis elegans*

INTRODUCTION

Clathrin-coated vesicles (CCVs) are major carriers of vesicular traffic in eukaryotic cells. In yeast, endocytosis involving clathrin is critically dependent on actin assembly, which provides motor activity as well as facilitates membrane invagination and vesicle scission (Sirotkin et al., 2005; Sun et al., 2006). In mammals, large GTPases of the dynamin family are the undisputed critical component for the fission of clathrin-coated pits (CCPs) from the plasma membrane (PM) (Ferguson and De Camilli, 2012). Nevertheless, prior studies using cultured cells have suggested that the actin-related protein 2/3 (Arp2/3) complex-activated actin filament assembly provides the force for membrane deformation under certain circumstances (Kirchhausen, 2009; Mooren et al., 2012). As a result, actin engagement was thought to be necessary for membranes to invaginate into coated pits only when cells are firmly attached to the substrate or when the membrane is under tension, such as at the apical surfaces of polarized cells (Gottlieb et al., 1993; Jackman et al., 1994; Da Costa et al., 2003; Hyman et al., 2006; Boulant et al., 2011).

Extensive efforts have been made to determine the functions of the actin assembly and to identify the interacting partners engaged in the actin assembly for CCP scission both *in vitro* and *in vivo* (Kessels et al., 2001; Gu et al., 2010). Bin-Amphiphysin-Rvs161/167 (BAR) domain-containing proteins coordinate with actin and tubulate the neck of coated pits before dynamin assembles to promote fission (Ferguson et al., 2009). A study using live-cell imaging has further revealed a reciprocal regulatory interaction between dynamin and actin at the membrane scission site: dynamin regulates actin recruitment and, in turn, becomes further stabilized by the actin assembly (Taylor et al., 2012). However, the recruitment, regulation and functional interdependence of actin and dynamin during this process remain only partly understood (Ferguson et al., 2009; Boulant et al., 2011; Taylor et al., 2012). An important, but challenging, task is to identify the specific domain(s) and interactions required for linking the actin assembly to endocytic sites.

To date, the Arp2/3 complex is the only nucleator of actin filaments found at endocytic sites (Mooren et al., 2012). To nucleate new branched actin networks, a nucleation-promoting factor (NPF) is necessary to induce a major conformational change in the Arp2/3 complex and to bring the actin-like Arp2 and Arp3 subunits into a configuration that mimics the barbed end of an actin filament (Rodal et al., 2005; Mooren et al., 2012). The Wiskott–Aldrich syndrome protein (WASP, also known as WAS) and its more widely expressed homolog, neural WASP (N-WASP, also known as WASL), are the proposed Arp2/3 NPFs involved in mammalian clathrin-mediated endocytosis (CME) (Merrifield et al., 2004). WASP-interacting protein (WIP, also known as WIPF1) is a WASP-binding partner (de la Fuente et al., 2007) that regulates WASP/N-WASP activity (Martinez-Quiles et al., 2001). Cumulative evidence has indicated that WIP may facilitate efficient actin polymerization independently of WASP via direct binding to actin (Martinez-Quiles et al., 2001; Anton et al., 2003; Ramesh et al., 2014) or via interaction with multiple actin regulators, such as Nck, profilin, cortactin and Abp1 (also known as Dbnl; DBN-1 in *Caenorhabditis elegans*) (Fried et al., 2014; Cortesio et al., 2010). A WASP-independent regulation of actin by WIP is involved in several cellular processes, including fibroblast focal adhesion assembly, T cell chemotaxis and migration, and membrane protrusion (Ramesh et al., 2014; Massaad et al., 2014).

[1]Key Laboratory of Molecular Biophysics of the Ministry of Education, College of Life Science and Technology, Huazhong University of Science and Technology, Wuhan, Hubei 430074, China. [2]National Laboratory of Biomacromolecules, Institute of Biophysics, Chinese Academy of Sciences, Beijing 100101, China. *Present address: Department of Organismic and Evolutionary Biology, Center for Brain Science, Harvard University, Cambridge, MA 02138, USA. ‡Present address: Department of Biochemistry and Molecular Biology, School of Basic Medicine and the Collaborative Innovation Center for Brain Science, Tongji Medical College, Huazhong University of Science and Technology, Wuhan, Hubei 430030, China. §These authors contributed equally to this work

¶Authors for correspondence (ryzhang@mail.hust.edu.cn; xutao@ibp.ac.cn)

T.X., 0000-0001-6436-6851; R.Z., 0000-0001-8969-5088

Received 28 November 2018; Accepted 13 May 2019

Journal of Cell Science (2019) 132, jcs228023. doi:10.1242/jcs.228023

However, our understanding of the WASP-independent functions of WIP remains limited; for example, we do not know whether this WASP-independent regulation of actin is involved in CCV generation.

Abp1, a highly conserved actin-binding protein, is involved in the functions of actin cytoskeleton during endocytosis in yeast and mammalian cells (Qualmann and Kessels, 2002; Engqvist-Goldstein and Drubin, 2003; He et al., 2015). Yeast Abp1 is a class II NPF that stimulates the nucleation of the Arp2/3 complex by strengthening its association with the sides of preexisting actin filaments (Welch and Mullins, 2002). However, studies of mammalian (m)Abp1 do not support a NPF function as in yeast (Kessels et al., 2000). The C-terminal Src homology 3 (SH3) domain of mAbp1 binds to proteins involved in endocytosis, such as synaptojanin 1, synapsin 1 and dynamin, perhaps allowing mAbp1 to functionally regulate endocytosis (Kessels et al., 2001; Mise-Omata et al., 2003). Hence, it remains unclear how Abp1 regulates the endocytosis process.

This study aims to elucidate the mechanism through which the actin assembly is coupled to endocytic sites. A small-scale screen was performed in *C. elegans* to identify candidate proteins whose knockdown potentially changes the steady-state distribution of the well-established clathrin-dependent cargo protein GFP-tagged human transferrin receptor (hTfR::GFP), in the intestines (Chen et al., 2006). Well-established genetic techniques and *in vivo* time-lapse microscopic approaches have made *C. elegans* intestine an efficient system for investigating the mechanisms underlying internalization, post-endocytic trafficking and cytoskeletal regulation in the context of multicellular organisms (McGhee, 2007; Grant et al., 2001; Chen et al., 2006; Shi et al., 2007, 2010). Here, we found that loss of the *C. elegans* homolog of WIP (WIP-1), the homolog of Abp1 (DBN-1) or components of the Arp2/3 complex resulted in the formation of aberrant tubular endocytic intermediates arrested at the basolateral intestinal membrane compared with the vesicles in the wild-type animals, as with inactivation of Dynamin-1 (DYN-1). However, the depletion of canonical class I NPFs [WASP (WSP-1), and WAVE/SCAR or WASH components] did not produce the aberrant tubular endocytic intermediates phenotype. Moreover, the recycling regulator RME-1 is required for the tubular endocytic intermediates phenotype caused by disruption of F-actin assembly. We also identified the interaction interfaces underlying the actin assembly and recruitment of DYN-1. Our study provides new insights into the molecular networks involved in actin function during CCV generation.

RESULTS

WIP-1 is required for endocytosis in the *C. elegans* intestine independently of WSP-1

C. elegans intestine carrying the hTfR::GFP fusion protein has been successfully used for studying mechanisms of CME and post-endocytic trafficking (Chen et al., 2006). In wild-type intestines, the transmembrane protein hTfR::GFP has a punctate localization pattern and is evenly distributed both on the basolateral membrane (top layer) and deep in the cytosol (middle layer) (Fig. 1A). Remarkably, intestines from animals with the null WIP-1 allele *wip-1*(*ok2435*) showed prominent basolateral accumulation of hTfR::GFP in tubular structures capped by the CCPs, and decreased numbers of puncta in the cytoplasm (Fig. 1A; Fig. S1A). Compared with the wild-type, the fluorescence intensity ratio of the basolateral to cytoplasmic hTfR::GFP increased by ∼4.3-fold, while the proportion of cytoplasmic hTfR-containing endosomes decreased to ∼20% (Fig. 1B,C), indicating an endocytosis defect arising from the null *wip-1*(*ok2435*) allele (Fig. 1D). Live-imaging results further demonstrated that the dynamic and short-lived hTfR::GFP spots of signal in the wild-type basolateral intestinal membrane became immobilized in *wip-1*(*ok2435*) mutants (Fig. S1B,C).

WIP-1 is the *C. elegans* homolog of WIP, which regulates the function of WASP/N-WASP in Arp2/3-mediated actin polymerization (Martinez-Quiles et al., 2001; Sawa and Takenawa, 2006). We next sought to identify whether the endocytosis defect is similarly induced by loss of WSP-1, the *C. elegans* WASP/N-WASP ortholog (Sawa and Takenawa, 2006). Surprisingly, both the morphology and distribution of hTfR::GFP signals were unaltered in homozygotes with a *wsp-1*-null allele (*gm324*) or deletion allele (*tm2299*) (Fig. 1A–C; Fig. S1D,E), indicating that the aberrant surface accumulation of hTfR induced by the loss of WIP-1 does not require WSP-1. WIP-1 contains two WASP homology 2 domains [WH2; the first WH2 at amino acids (aa) 28–55; second WH2, at aa 83–99], one cortactin-binding domain (CBD; aa 118–174) within a proline-rich region, and one WSP-1-binding domain (WBD; aa 338–362) (Fig. 1E) (Fried et al., 2014; Sawa and Takenawa, 2006). Notably, in the *wip-1*(*ok2435*) intestinal epithelium, transgenic expression of a full-length WIP-1 (RFP::WIP-1) and fragment of WIP-1 missing the WBD domain [WIP-1(ΔWBD)] driven by the intestine-specific promoter completely rescued the over accumulation of hTfR::GFP in the aberrant tubular structures (Fig. 1B,C,F). This result further suggests that WIP-1–WSP-1 interaction is dispensable to the defect in hTfR endocytosis.

To verify that the endocytosis defect induced in the *wip-1* mutant is not specific to the exogenously expressed hTfR, we further examined the localization of the Wntless ortholog MIG-14, another clathrin-dependent endocytic cargo protein that is retrograde transported to the Golgi (Pan et al., 2008; Shi et al., 2009). As observed for hTfR::GFP, MIG-14::GFP also over accumulated in tubular carriers at the basolateral intestinal membrane in *wip-1*(*ok2435*) mutants, and showed a comparable number of puncta in *wsp-1(gm324)* mutants to that in the wild-type intestines (Fig. 1G). This suggests that WIP-1 function in CME in the *C. elegans* intestine is independent of WSP-1.

In addition to WASP/N-WASP, the WAVE/SCAR and WASH complexes also act as Arp2/3 NPFs (Patel and Soto, 2013). To examine their involvement in CCV generation, RNAi feeding was performed to deplete each member of WAVE/SCAR (*wve-1*, *gex-2*, *gex-3*, *abi-1* or *nuo-3*) (Patel and Soto, 2013) and WASH complexes (*ddl-2*, *Y53F4B.21*, *T05E7.3*, *C06A8.8* or *ddl-1*) (Bai, 2015). The effect of RNAi was confirmed by detecting the mRNA levels through quantitative real-time reverse-transcription PCR (qRT-PCR) (Fig. S2A,C). RNAi of the individual genes of the WASH complex did not change the distribution of hTfR::GFP puncta; however, depletion of the WAVE/SCAR components resulted in an accumulation of hTfR-positive puncta at the basolateral intestinal membrane (Fig. S2). These data are consistent with previous reports showing that WAVE/SCAR also participates in cargo transport from the PM to early endosomes during CME (Patel and Soto, 2013). Taken together, our results demonstrate that WIP-1 is required for CME in the intestine of *C. elegans*. Moreover, this function of WIP-1 is independent of WSP-1.

WIP-1 regulates the generation of endocytic vesicles by engaging actin filaments and DBN-1

In addition to regulating WASP/N-WASP function in Arp2/3-mediated actin polymerization, WIP directly binds to G- and F-actin through its first WH2 domain and is capable of binding to a number of actin polymerization regulators by the virtue of its high proportion

Journal of Cell Science (2019) 132, jcs228023. doi:10.1242/jcs.228023

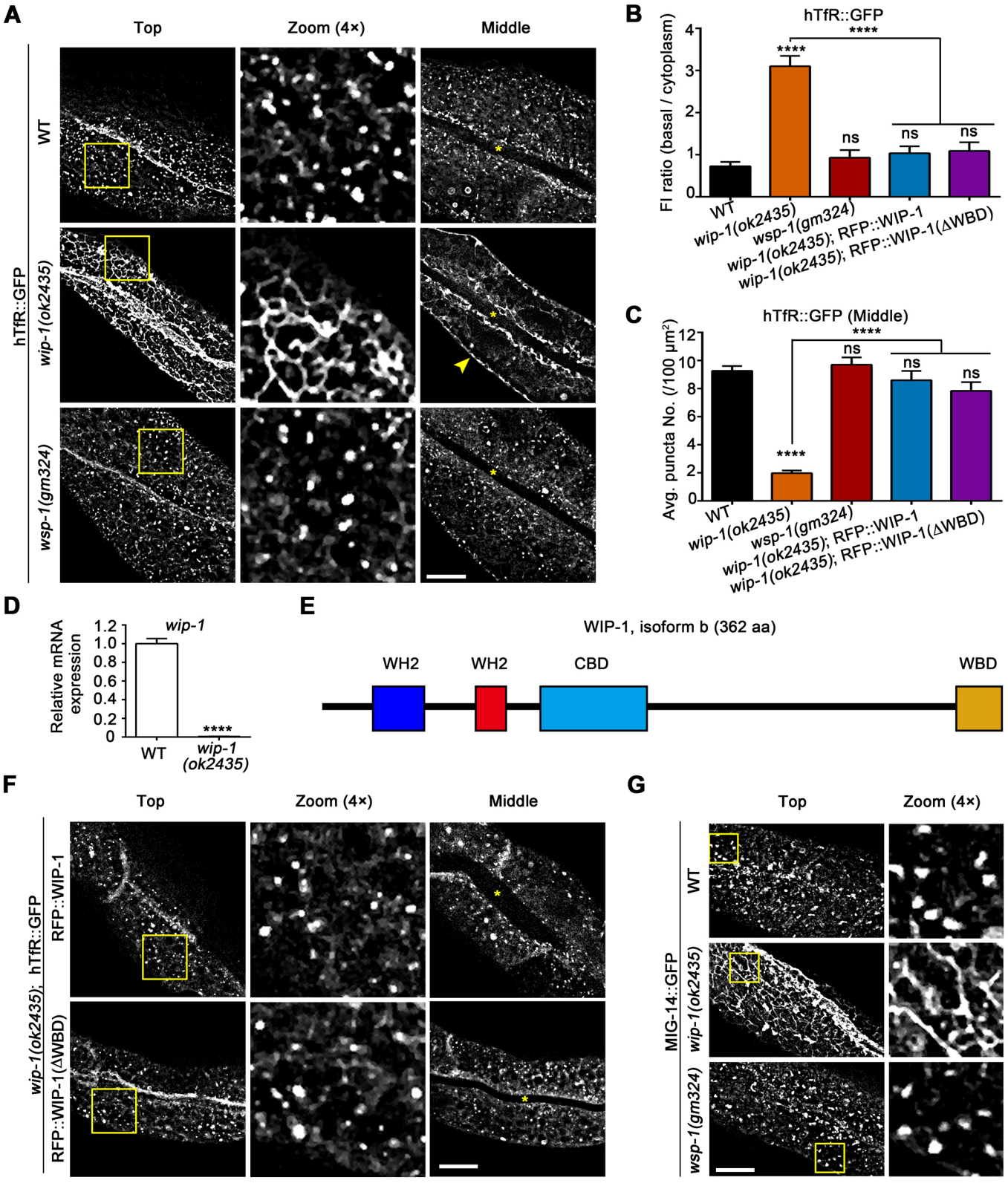

Fig. 1. See next page for legend.

of proline residues (Anton and Jones, 2006). Treatment with latrunculin B (LatB), an actin monomer-sequestering agent, which blocks the fast polymerization of actin (Spector et al., 1983), or knockdown of the Arp2/3 complex component ARX-2 (see mRNA in Fig. 2E), resulted in the abnormal accumulation of hTfR::GFP in tubular structures at the basolateral intestinal membrane (Fig. 2A), as with the *wip-1*(*ok2435*) mutant intestines. Moreover, overexpression of WIP-1 with a deletion of the first WH2 domain [WIP-1(Δ1st WH2)] failed to rescue hTfR::GFP endocytosis defects in *wip-1*(*ok2435*) mutants (Fig. 2B–D). We postulate that WIP-1 may affect

Journal of Cell Science (2019) 132, jcs228023. doi:10.1242/jcs.228023

Fig. 1. *C. elegans* WIP-1 is required for internalization of various clathrin-dependent cargo proteins independent of WSP-1. (A) Micrographs taken with an 150× objective showing the detailed distribution and architectures for intestinal hTfR::GFP signals in wild-type (WT), *wip-1(ok2435)* or *wsp-1(gm324)* mutants. The middle column (Zoom) shows enlargements of the indicated areas. The arrowhead indicates basolateral PM-associated hTfR::GFP. Asterisks depict the intestine lumen. (B,C) The basolateral membrane to cytoplasmic (basal/cytoplasm) fluorescence intensity (FI) ratio of hTfR::GFP (B) and the number of cytoplasmic puncta positive for hTfR::GFP (C) were calculated for intestines of each indicated genotype. *n*=20 regions from 20 animals for each condition. Data are mean±s.e.m. from three independent experiments, performed in duplicate. ns, not significant; ****P<0.0001 (one-way ANOVA). (D) qRT-PCR analysis of *wip-1* gene expression from total RNAs from the WT and *wip-1(ok2435)* animals. Data are mean±s.e.m. from three independent experiments. ****P<0.0001 (*t*-test). (E) Domain architecture of WIP-1 isoform b. (F) Confocal images show the hTfR::GFP endocytosis complementing effect of the RFP::WIP-1 fragments in *wip-1(ok2435)* mutants. Overexpression of either the full-length or the WBD-deleted WIP-1 leads to successful recovery of the distribution and punctate morphology of hTfR signals. (G) Representative confocal images showing another clathrin-dependent endocytic cargo, MIG-14, at the basolateral membrane in WT, *wip-1(ok2435)* and *wsp-1(gm324)* mutants. Top refers to the basolateral surface of the intestine, and Middle indicates a cross-section of the intestine. Scale bars: 10 µm.

the production of hTfR-containing endocytic vesicles by influencing Arp2/3-nucleated actin filaments.

C. elegans DBN-1 is a member of the Abp1/drebrin class of actin-binding proteins (Butkevich et al., 2015). Previous studies on mammalian cells have suggested mAbp1 functions in dorsal ruffle formation by binding to the CBD domain of WIP (Cortesio et al., 2010; Fried et al., 2014). We next examined the impact of DBN-1 on hTfR endocytosis. Notably, a similar endocytosis defect was observed in *dbn-1*-depleted intestines to that seen with loss of WIP-1 (Fig. 2A). To gain insight into the functional relationship between DBN-1 and WIP-1 in CME, we examined the effect of the CBD domain on the *wip-1*(*ok2435*)-induced hTfR endocytosis defect. Our results show that transgenic expression of WIP-1 without a CBD [WIP-1(ΔCBD)] failed to restore hTfR endocytosis in *wip-1*(*ok2435*) mutants (Fig. 2B–D), indicating that WIP-1 regulation of CME is likely mediated by DBN-1.

Next, we examined subcellular localization of WIP-1 and DBN-1 *in vivo*. Live-cell imaging revealed a significant overlap between the GFP::WIP-1 and RFP::DBN-1 localization in punctate structures at the basolateral intestinal membrane (Fig. 2F). Moreover, in *wip-1*(*ok2435*) mutants, the number of RFP::DBN-1 puncta decreased by 70% and few of the remaining puncta overlapped with the arrested hTfR::GFP tubules (Fig. 2G,H). Expression of the GFP::WIP-1(ΔCBD) construct consistently gave rise to severely attenuated RFP::DBN-1 signals at the basolateral intestinal membrane (Fig. S3). In contrast, DBN-1 loss induced only a slight increase in the number of RFP::WIP-1 puncta (∼35%) (Fig. 2I). Taken together, these results imply that WIP-1 contributes to the localization of DBN-1 at endocytic sites.

Actin assembly cooperate with DYN-1 for the scission of CCPs

The aforementioned arrested hTfR::GFP-containing tubule is reminiscent of the ineffective fission of CCPs seen when the GTPase dynamin is inactive (Ferguson et al., 2009; Itoh et al., 2005). To test this assumption, we examined the effect of DYN-1 on hTfR::GFP endocytosis by analyzing animals with a temperature-sensitive mutation, *dyn-1(ky51)* (Clark et al., 1997). At the restrictive temperature of 25°C, *dyn-1*(*ky51*) mutant intestines consistently displayed prominent accumulation of hTfR-containing tubules at the basolateral intestinal membrane, with significantly fewer puncta in the cytoplasm (Fig. 3A), as observed in *wip-1*(*ok2435*) mutants. Endocytosis was successfully rescued by the expression of DYN-1::RFP driven by the intestinal promoter *vha-6* (Fig. 3A–C). The similar phenotype caused by disrupting actin assembly to that seen upon inactivation of DYN-1 indicates that scission defect is the cause of the tubular endocytic intermediates phenotype.

We then proceeded to verify that the aberrant accumulation of clathrin cargo proteins, such as hTfR::GFP, indeed depicts the defective endocytic intermediates emanating from the PM due to abortive scission. Our previous work reported that fluorescent 10 kDa dextran (Dex10) is able to enter cells through clathrin- and dynamin-dependent micropinocytosis in addition to macropinocytosis (Li et al., 2015). Moreover, the basolaterally internalized Dex10 follows a fast recycling pathway to recycle back into the pseudocoelom, where it is finally taken up by coelomocytes, the scavenger cells located in the pseudocoelom of *C. elegans* (Chen et al., 2014; Fares and Greenwald, 2001). We assessed the uptake of Rhodamine-conjugated dextran (Rhod–dextran) microinjected into the pseudocoelom (Fig. 3D; Fig. S4). As expected, in wild-type worms, the fast recycling profile prevented the basolaterally internalized Dex10 from overlapping with the surface-localized hTfR::GFP. However, in *wip-1(ok2435)* and *dyn-1(ky51)* mutants, the Dex10 signals were prominently positive for hTfR::GFP in tubular structures at the basolateral intestinal membrane. This result strongly suggested that the hTfR-positive tubules represent the membranous tubules extending from the PM due to aborted endocytic scission.

Furthermore, we sought to investigate the recruitment of and functional relationship between the assembled actin and DYN-1. We examined the subcellular localization of RFP-tagged WIP-1, DBN-1 and ARX-2 with respect to DYN-1::GFP. Substantial colocalization was observed for each group (Fig. 3E,F; mean±s.e.m. Pearson's coefficient: WIP-1, 78.3±1.7%; DBN-1, 83.1±1.8%; ARX-2, 79.2±1.9%, *n*=18 regions), implicating that these molecules function together. In addition, we demonstrated that DBN-1, the branched F-actin and clathrin colocalized with each other (Fig. S5), suggesting that WIP-1 and DBN-1 are involved in promoting F-actin polymerization at the membrane-associated CCP sites. Next, we monitored the effect of WIP-1 and DBN-1 loss on DYN-1 recruitment to the basolateral intestinal membrane. DYN-1::RFP levels decreased to ∼39% in *wip-1*(*ok2435*) and ∼21% in *dbn-1*(*ok925*) mutants compared with that in the wild-type (Fig. 3G). In contrast, the number of DBN-1 puncta on the basolateral intestinal membrane of *dyn-1*(*ky51*) increased marginally (∼1.7-fold) (Fig. 3H). Taken together, these findings suggest that the assembled actin filaments and DYN-1 act cooperatively for the scission of CCPs and that actin assembly contributes to the recruitment of DYN-1 (Grassart et al., 2014).

Interaction between DBN-1 and F-actin is important for DYN-1 recruitment during CCV generation

In *dbn-1*(*ok925*) mutants, Lifeact::GFP signals were obviously not from branched structures and less colocalized with CLIC-1::RFP, indicating that DBN-1 promotes F-actin polymerization at the CCP sites (Fig. S5C,D). DBN-1 is composed of an N-terminal actin depolymerizing factor homology (ADF-H) domain (aa 4–133), three isolated coiled-coil domains (3CC, aa 134–368), a proline-rich region (PRD, aa 369–584) and an SH3 domain (aa 585–643) (Fig. 4A) (Butkevich et al., 2015). To define the functional input of DBN-1 domains in CCV generation, we investigated the

Journal of Cell Science (2019) 132, jcs228023. doi:10.1242/jcs.228023

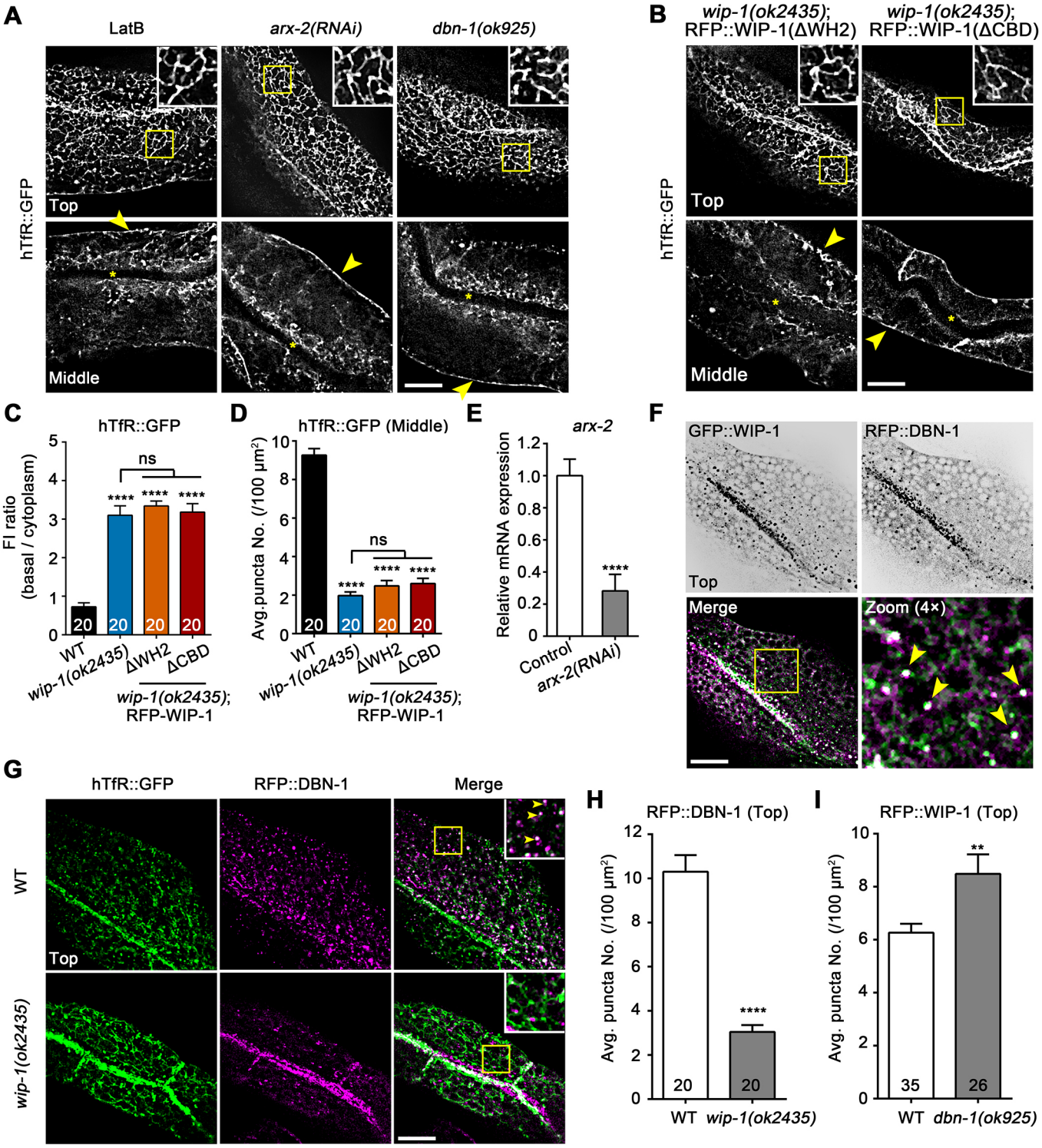

Fig. 2. See next page for legend.

complementary effect of various DBN-1 fragments in *dbn-1*(*ok925*) deletion allele mutants (Fig. 4B,D,E). Overexpression of a DBN-1 construct lacking either the ADF-H (ΔADF-H) or 3CC (Δ3CC) domain failed to restore punctate hTfR::GFP distribution. However, RFP::DBN-1(ΔPRD) and RFP::DBN-1(ΔSH3) constructs effectively restored punctate hTfR distribution, as with the wild-type DBN-1 construct, suggesting that actin binding is prerequisite for the DBN-1-mediated regulation of CCP scission.

To determine whether the recovery of punctate hTfR distribution is associated with DYN-1 recruitment to endocytic sites, we examined the effect of DBN-1 fragment overexpression on DYN-1::GFP localization. Correlating with the recovery effect, both RFP::DBN-1(ΔADF-H) and RFP::DBN-1(Δ3CC) resulted in severely attenuated DYN-1::GFP signals, whereas expression of DBN-1 lacking either the PRD or SH3 domain did not visibly alter punctate DYN-1::GFP distribution at the basolateral intestinal

Journal of Cell Science (2019) 132, jcs228023. doi:10.1242/jcs.228023

Fig. 2. WIP-1 regulates CME through actin filaments and DBN-1. (A) Confocal images showing tubular structures with accumulated hTfR::GFP at the basolateral membrane and diminished punctate signals in the cytoplasm of intestines after treatment with LatB, *arx-2* RNAi or in *dbn-1*(*ok925*) animals. (B) Overexpression of the fragments RFP::WIP-1(Δ1st WH2) or RFP::WIP-1(ΔCBD) in *wip-1(ok2435)* mutant intestines did not recover the defective endocytosis of hTfR::GFP. Arrowheads in A and B indicate basolateral PM-associated hTfR::GFP. Asterisks depict the intestine lumen. (C,D) The basolateral membrane to cytoplasm (basal/cytoplasm) fluorescence intensity (FI) ratio of hTfR::GFP (C) and the puncta density of hTfR::GFP in the cytoplasm (D) were quantified for intestines of each indicated genotype. WT, wild-type. (E) qRT-PCR analysis to show the RNAi silencing efficiency for the *arx-2* gene. Data are mean±s.e.m. from three independent experiments. ****P<0.0001 (*t*-test). (F) Confocal images showing colocalization between GFP::WIP-1 and RFP::DBN-1 at the basolateral membrane of wild-type intestines. Arrowheads indicate positive overlap. (G) Confocal images of the intestinal basolateral membrane in hTfR::GFP worms expressing RFP::DBN-1 in wild-type or *wip-1(ok2435)* mutant animals. Arrowheads indicate positive overlap. (H,I) Quantification of the number of RFP::DBN-1 puncta in *wip-1(ok2435)* mutants (H) and RFP::WIP-1 puncta in *dbn-1*(*ok925*) mutants (I). In A, B, F and G, the insets are magnified views of the boxed areas. Scale bars: 10 µm. In C, D, H and I, the number of areas analyzed for each group is indicated in each bar; at least 20 animals were analyzed for each group. Data are mean ±s.e.m. from three independent experiments. In C and D, ns, not significant; ****P<0.0001 (one-way ANOVA). In H and I, **P=0.004; ****P<0.0001 (Mann–Whitney test). Top refers to the basolateral surface of the intestine, and Middle indicates a cross-section of the intestine.

membrane (Fig. 4C,F). Thus, although the function of DBN-1 in CCV generation is linked to DYN-1, our data do not support an indispensable role for the SH3 domain of DBN-1 in recruiting DYN-1 to the endocytic sites. By contrast, the interactions with F-actin through both ADF-H and 3CC domains are important for DYN-1 recruitment to endocytic sites.

The EHD-containing protein RME-1 stabilizes the elongated endocytic vesicles

To better characterize the arrested hTfR-containing tubules, we examined the early and basolateral recycling endosomes by using fluorescently tagged RAB-5 and RME-1, respectively. As expected, the defective endocytosis in *wip-1(ok2435)* and *dbn-1(ok925)* mutants resulted in the hTfR-positive tubules having less RFP::RAB-5 (Fig. S6). Surprisingly, we found that the arrested hTfR-containing tubules in *arx-2*(*RNAi*), *dbn-1(ok925)*, and *dyn-1*(*ky51*) worms displayed significantly increased RME-1 labeling [mean ±s.e.m. Pearson's coefficient: *arx-2*(*RNAi*), 0.63±0.02; *dbn-1(ok925)* 0.71±0.03; *dyn-1*(*ky51*), 0.68±0.02; n=20 regions] compared with control worms (mean±s.e.m. Pearson's coefficient: 0.42±0.02; n=20 regions) (Fig. 5A,B). As the only member of Eps15 homology (EH) domain-containing proteins (EHDs) in *C. elegans*, RME-1 has been proposed to function by promoting molecule recycling from endosomes back to the cell surface and is observed in tubulo-vesicular structures near the basolateral intestinal membrane (Fig. 5A) (Grant et al., 2001). As a control, we analyzed the effect of disrupting CCP initiation on hTfR::GFP colabeling with RME-1. As expected, depletion of clathrin by means of RNAi (*chc-1 RNAi*, mRNA in Fig. 5C) increased the number of hTfR puncta at the basolateral intestinal membrane, which were negative for RME-1 (mean±s.e.m. Pearson's coefficient: 0.26±0.02; n=20 regions) (Fig. 5A,B). Taken together, these findings support the idea that the recycling factor RME-1 is increasingly recruited to the tubular hTfR::GFP-containing endocytic intermediates but not to the clustered hTfR proteins on the PM.

Next, we analyzed hTfR distribution in *rme-1*(*b1045*); *dbn-1(ok925)* and *rme-1*(*b1045*); *dyn-1*(*ky51*) double-mutant worms (Fig. 5D). *b1045* is a deletion allele of *rme-1* (Grant et al., 2001). Surprisingly, the deletion mutant of *rme-1* produced distinct effects on the scission defect induced in *dbn-1(ok925)* or *dyn-1*(*ky51*) mutants. In *rme-1*(*b1045*); *dbn-1(ok925)* double mutants, the formation of hTfR::GFP-containing endocytic tubules was substantially reduced, and punctate hTfR signals reappeared at the basolateral intestinal membrane (mean±s.e.m. average puncta number: *dbn-1(ok925)*, 5.965±0.367; *rme-1*(*b1045*); *dbn-1(ok925)*, 11.871±0.839; n=18 regions), while in the cytoplasm, hTfR::GFP puncta were also visible, albeit to a lower extent than in the wild-type worms (mean±s.e.m. average puncta number: wild-type, 7.933±0.356; *rme-1*(*b1045*); *dbn-1(ok925)*, 3.816±0.584; n=18 regions) (Fig. 5D–G). These data are reminiscent of results from previous studies of defective scission caused by disruption of actin assembly on mammalian cells, wherein CCPs are stalled on the plasma membrane and endocytosis is ceased (Boulant et al., 2011). However, here in our studies, because DYN-1 recruitment to endocytic sites was not fully blocked, a few hTfR::GFP puncta are visible in the cytoplasm. In contrast, the tubular morphology of hTfR::GFP seen in *dyn-1*(*ky51*) single mutants was not recovered at all in *rme-1*(*b1045*); *dyn-1*(*ky51*) double mutants (Fig. 5D–G), suggesting that F-actin polymerizes and generates force against the basolateral membrane, which supports the formation of tubular endocytic intermediates.

hTAC internalization is also affected by loss of WIP-1 or DBN-1 in the *C. elegans* intestine

As a comparison, we also examined the *C. elegans* carrying GFP-tagged hTAC (the α-chain of the human IL-2 receptor), a cargo protein that undergoes Arf6-dependent clathrin-independent endocytosis (CIE) (Radhakrishna and Donaldson, 1997). Most hTAC::GFP was found beneath the basolateral plasmalemma in the delicate tubulo-vesicular network, which was significantly labeled by RFP::RME-1 in wild-type as well as in *wip-1*(*ok2435*) and *dyn-1(ky51)* mutant worms (Fig. S7A,B). However, different from the wild-type hTAC tubules, the hTAC tubules in *wip-1*(*ok2435*) were strongly labeled by the Rhod–Dex pre-injected into the pseudocoelom (Fig. S7C). Moreover, to our surprise, in *wip-1(ok2435)* mutants, these hTAC tubules not only extensively overlapped with the aberrant MIG-14-containing tubules, but also were increasingly capped by clathrin (Fig. S7D–G). These results are reminiscent of a recent report (Zhu et al., 2018), in which Zhu et al. proposed that in mammalian cells hTAC is internalized by both the CIE and CDE pathways.

We then examined the endosomal localization of DBN-1. We found that a significant amount of DBN-1 localized at RAB-5-positive early endosomes, but very little showed colocalization with RAB-10-associated endosomes, RME-1-associated basolateral recycling endosomes or RAB-7-associated late endosomes (Fig. S7H,I). Gryaznova et al. have reported that WIP also localizes on RAB-4-positive endosomes (Gryaznova et al., 2018). Taken together, these results support that WIP-1 and DBN-1 do not play a profound role during the post-endocytic recycling or degradation pathway.

DISCUSSION

Accumulating evidence has indicated that actin and dynamin cooperate during CCP scission in eukaryotic cells. Molecular mechanisms underlying the spatio-temporal assembly of actin and dynamin during this process remain poorly understood. Here, we demonstrate in *C. elegans* that two actin-binding proteins, WIP-1 and DBN-1, mediate CCP scission by linking the actin assembly to

Journal of Cell Science (2019) 132, jcs228023. doi:10.1242/jcs.228023

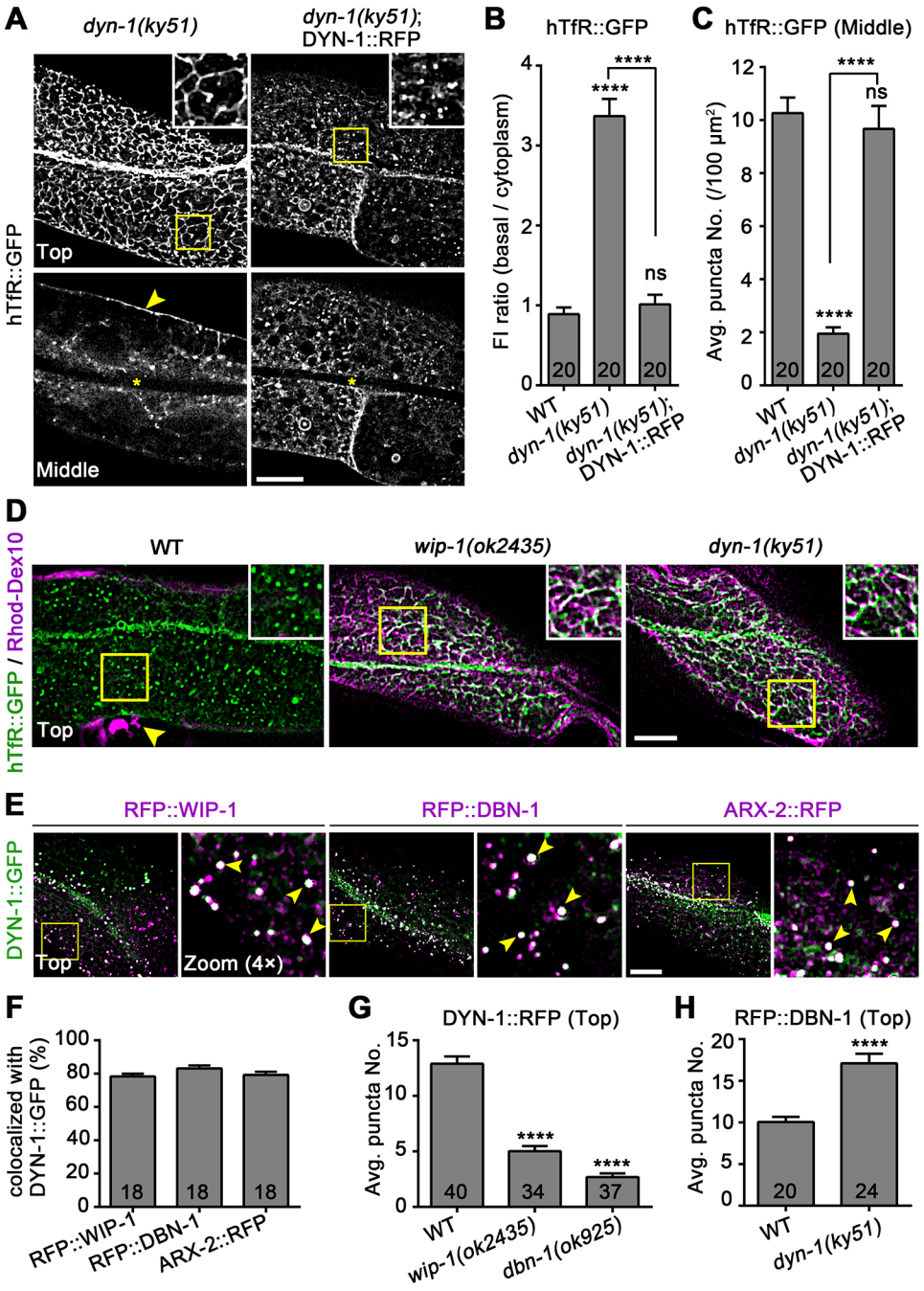

Fig. 3. The actin filaments cooperate with DYN-1 for scission of CCPs. (A) Confocal images showing the defect in endocytosis of hTfR::GFP in *dyn-1(ky51)* intestines at 25°C and the complementing effect of DYN-1::RFP. The arrowhead indicates basolateral PM-associated hTfR::GFP. Asterisks depict the intestine lumen. (B,C) The basolateral membrane to cytoplasm (basal/cytoplasm) fluorescence intensity (FI) ratio of hTfR::GFP (B) and the number of hTfR::GFP puncta in the cytoplasm (C) were calculated for intestines depicted in A. WT, wild-type. (D) Wild-type, *wip-1(ok2435)* and *dyn-1(ky51)* mutant intestines carrying hTfR::GFP are exposed to basolateral Rhod–Dex10. The arrowhead indicates coelomocyte with internalized Rhod–Dex10 in the wild-type animal. (E,F) Representative colocalization images (E) and quantification (%) (F) of RFP-tagged WIP-1, DBN-1 or ARX-2 with DYN-1::GFP at the basolateral membrane. Insets show the enlargement of the indicated areas. Arrowheads indicate positive overlap. (G) Quantification of the number of DYN-1::RFP dots at the basolateral membrane in wild-type, *wip-1(ok2435)*, or *dbn-1(ok925)* mutant intestines. (H) Quantification of the number of RFP::DBN-1 dots at the basolateral membrane in wild-type or *dyn-1(ky51)* mutant intestines at 25°C. The number of areas analyzed for each group is indicated in each bar. At least 18 animals were analyzed for each group. Data are mean±s.e.m. from three independent experiments. In B, C and G, ns, not significant; ****P<0.0001 (one-way ANOVA). In H, ****P<0.0001 (Mann–Whitney). In A, D and E, the insets are magnified view of the boxed areas. Top refers to the basolateral surface of the intestine, and Middle indicates a cross-section of the intestine. Scale bars: 10 µm.

DYN-1. Moreover, we demonstrate for the first time that the arrested tubular endocytic intermediates originating from either impairment of F-actin assembly or inactivation of the GTPase DYN-1, were increasingly labeled by RME-1.

The results of our study are summarized in the model shown in Fig. 6. At endocytic sites, membrane-curvature-sensing BAR/F-BAR proteins initiate membrane tubulation (Itoh et al., 2005; Ferguson et al., 2009). With the assistance of F-actin assembly forcing against the membrane, fission mediated by DYN-1 results in CCV generation. Loss of either force-generating F-actin assembly or the GTPase DYN-1 means that BAR/F-BAR-initiated membrane tubules are not efficiently sheared, and the aberrant RME-1 association further stabilizes the tubules and attenuates the scission. In mutant worms with simultaneous loss of RME-1 and DBN-1, endocytosis is still diminished to a significant level due to the loss of force-generating F-actin as well the attenuated DYN-1 recruitment at endocytic sites, but the majority of endocytic intermediates are punctate instead of tubular, as observed upon F-actin disruption in MDCK cells (Boulant et al., 2011). By contrast, in mutant worms with simultaneous loss of RME-1 and DYN-1, F-actin assembly forces the membranous tubules against the PM, as observed for dynamin 1 and 2 double-knockout in fibroblast cells (Ferguson et al., 2009). Together, these findings support the idea that fission mediated by DYN-1 plays an essential role in the scission step during CME. F-actin assembly kinetically facilitates scission by forcing the BAR/F-BAR-initiated tubules away from the membrane.

Membrane remodeling occurs through the complex interplay between membrane proteins, lipids and physical forces applied to the membrane surface. Presently, we do not know how the lipid components or membrane tension of the *C. elegans*

Journal of Cell Science (2019) 132, jcs228023. doi:10.1242/jcs.228023

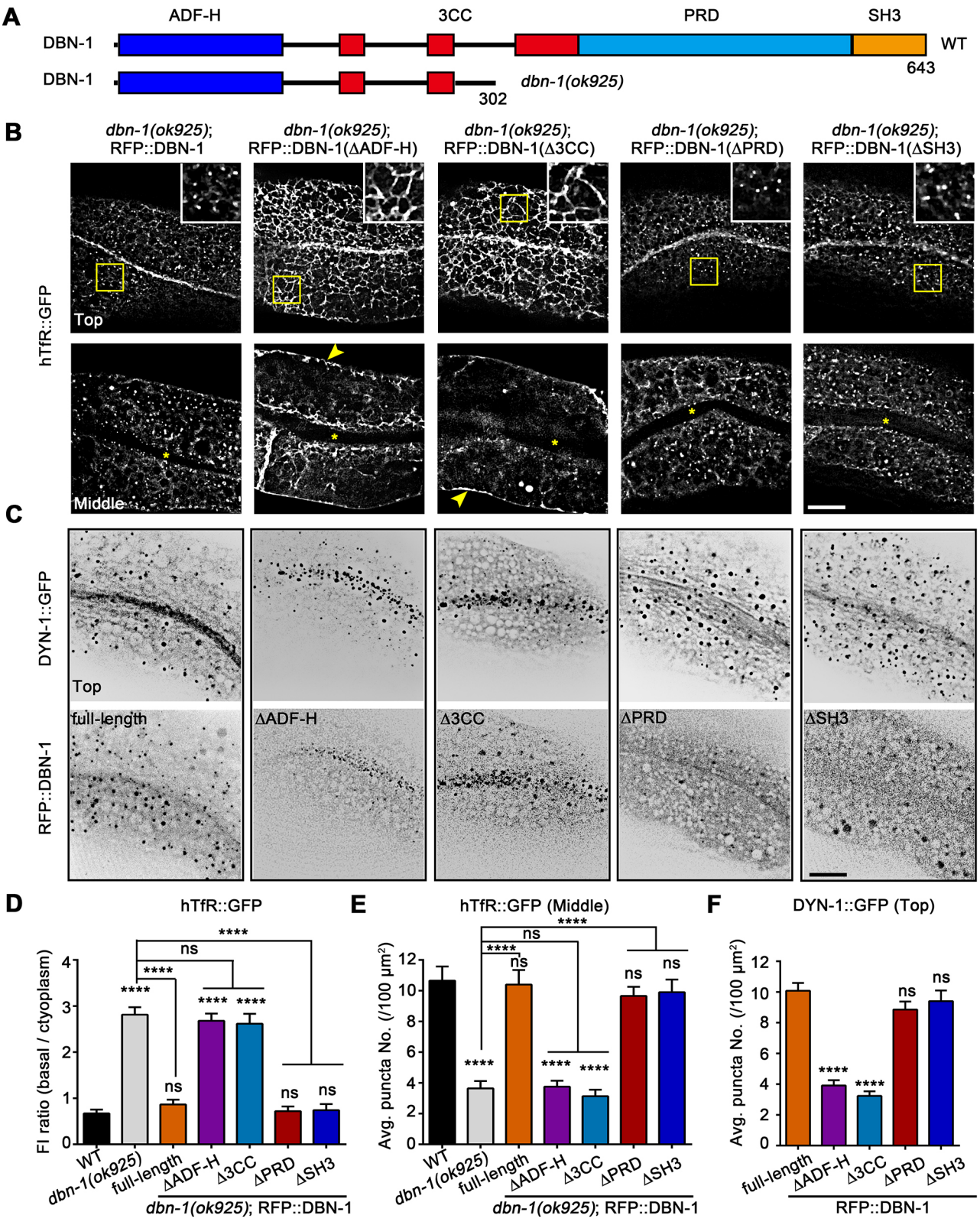

Fig. 4. See next page for legend.

intestine responds to the attenuated scission of BAR-induced membrane tubules, or how RME-1 is aberrantly recruited to and further stabilizes the tubules but does not promote fission. Further research is needed to explore these questions. Moreover, we note that, during the preparation of the manuscript, Deo et al. (2018) reported that the conventionally used N-terminal tagging of EHD proteins probably causes enhanced basolateral ATPase activity compared with WT EHD proteins and influences their

Journal of Cell Science (2019) 132, jcs228023. doi:10.1242/jcs.228023

Fig. 4. F-actin–DBN-1 binding is a prerequisite for recruitment of DYN-1 to endocytic sites and final CCP scission. (A) Schematic representations of DBN-1 in wild-type (WT, upper) and *dbn-1(ok925)* mutant animals (lower). (B) Confocal images show the hTfR::GFP endocytosis complementing effect of the RFP::DBN-1 fragments in *dbn-1(ok925)* mutants. Arrowheads indicate basolateral PM-associated hTfR::GFP. Asterisks depict the intestine lumen. The insets are a magnified view of the boxed areas. (C) Confocal images showing the effect of DBN-1 truncations on the DYN-1::GFP localization at the basolateral membrane. Truncations deleting either ADF-H, 3CC, PRD or SH3 domains influenced DBN-1 localization to the basolateral membrane, but only those deleting ADF-H or 3CC domain disturbed the DYN-1 localization to the endocytic sites. (D,E) The basolateral membrane to cytoplasm (basal/cytoplasm) fluorescence intensity (FI) ratio of hTfR::GFP (D) and the puncta density of hTfR::GFP in the cytoplasm (E) were calculated for intestines depicted in B. (F) The puncta density of DYN-1::GFP at the basolateral membrane was calculated for intestines depicted in C. n=20 regions from 20 animals for each group in D–F. Data are mean±s.e.m. from three independent experiments. ns, not significant; ****P<0.0001 (one-way ANOVA). Top refers to the basolateral surface of the intestine, and Middle indicates a cross-section of the intestine. Scale bars: 10 µm.

oligomerization interface. We think that in the future it will be helpful to further verify whether the cellular function of RME-1 is interfered with when adding N- or C-terminally fused fluorescent tags.

The Arf6-dependent CIE cargo protein hTAC normally transports via the tubular subplasmalemma recycling endosomes along the recycling pathway (Chen et al., 2014). To our surprise, the *wip-1(ok2435)*-induced aberrant membranous tubules contained both the CIE cargo hTAC and the CDE cargoes hTfR and MIG-14, and were capped by the CCPs at the tubular tips. Considering that WIP-1 and DBN-1 localize mainly at the CCPs and early endosomes, but not recycling endosomes and late endosomes (Gryaznova et al., 2015; Gryaznova et al., 2018; He et al., 2015), we inferred from the assay of Rhod–Dex staining that these membranous tubules are surface-connected scission-defective endocytic intermediates. However, we cannot exclude other possibilities, such as the F-actin dynamic assembly regulated by WIP-1 and DBN-1 at the early endosomes having an effect on the post-endocytic protein sorting or loss of WIP-1 or DBN-1 resulting in shunting of the CDE cargoes into RME-1-associated tubular subplasmalemma recycling endosomes as the CIE cargoes.

Our study also provides new insights into the molecular network that underlies actin participation in the scission of CCVs. WASP-independent regulation of actin by WIP was reported to function in cell adhesion and migration and to stimulate the formation of membrane protrusions (Ramesh et al., 2014; Massaad et al., 2014). Herein, we demonstrate for the first time that WIP-1 is involved in the actin-regulated scission of CME independently of WSP-1. Consistent with our findings, a previous study on *C. elegans* has reported that intestines depleted of *wsp-1* had a CME capability that was comparable to that of wild-type intestines (Patel and Soto, 2013). Moreover, in addition to the previous report that WIP and mAbp1 cooperate for dorsal ruffle formation (Cortesio et al., 2010), we demonstrate that DBN-1 (the homolog of mAbp1) acts as an interacting partner with WIP-1 during CCP scission, and the localization of DBN-1 to endocytic sites is facilitated by WIP-1. Studies on mammalian cells have suggested that mAbp1 functionally regulates endocytosis through the binding of dynamin proteins to its C-terminal SH3 domain (Kessels et al., 2001; He et al., 2015). However, our data do not support the functional importance of this interaction. By contrast, abolition of the two independent F-actin-binding modules (i.e. the N-terminal ADF-H and the central helical domain) results in severely decreased numbers of DYN-1 puncta at the basolateral intestinal membrane and aberrant hTfR::GFP endocytosis, strongly suggesting that F-actin plays a critical and direct role in recruiting DYN-1 (Taylor et al., 2012).

Together, our data support the model depicted in Fig. 7. At endocytic sites, WIP-1 promotes actin polymerization by binding to G-actin and F-actin, and recruits DBN-1 through its CBD domain; DBN-1 further binds to F-actin through its ADF-H and the 3CC domains. The actin assembly then facilitates DYN-1 recruitment and acts cooperatively to promote CCP scission at endocytic sites. Nonetheless, how the Arp2/3 complex is activated to mediate actin polymerization remains a unanswered question. Patel and Soto (2013) have proposed that WAVE/SCAR, but not WSP-1, serves as an NPF in *C. elegans* intestines to mediate the activity of the Arp2/3 complex. In our study, the disruption of any individual component of NPFs did not result in the accumulation of aberrant tubular endocytic intermediates as in *wip-1*(*ok2435*) and *dbn-1(ok925)* mutants. One possibility is that DBN-1 serves to nucleate the Arp2/3 complex to mediate actin polymerization. Although previous studies on mAbp1 do not support this function (Kessels et al., 2000), yeast Abp1 and mammalian cortactin have been reported to be non-canonical NPFs (Welch and Mullins, 2002; Helgeson et al., 2014). In conclusion, our results support that F-actin and DYN-1 act coordinately to mediate CCP scission in the *C. elegans* intestine, and we further identified a novel role for WIP-1 and DBN-1 in regulating F-actin assembly at the endocytic sites and cooperating with DYN-1 by identifying their mutual interaction interfaces. Further studies will be necessary to understand the mechanism underlying Arp2/3 complex activation.

MATERIALS AND METHODS

General methods and strains

All *C. elegans* strains were derived from the wild-type Bristol strain N2. Genetic crosses and husbandry methods were performed according to standard protocols described by Brenner (1974). A list of mutant and transgenic strains used in this study can be found in Table S1. Mutant animals were outcrossed with N2 five times to eliminate the background mutation and were confirmed by PCR and sequencing. Worms were cultured at 20°C on nematode growth medium (NGM) plates with *E. coli* OP50 for normal breeding. The temperature-sensitive allele *dyn-1(ky51)* animals were shifted to the restrictive temperature of 25°C as L4 stage and scored after 12 h for imaging (Clark et al., 1997). *C. elegans* RNAi-mediated interference was performed as described previously (Timmons and Fire, 1998). All bacterial RNAi feeding constructs were derived from the Ahringer library, controls were treated with bacterial strain HT115(DE3), which was transformed with empty L4440 feeding vector (Kamath et al., 2001). For most RNAi experiments, synchronized L1 stage worms were cultured for 60 h and scored as young adults. For *arx-2* and *chc-1* RNAi, synchronized L3 stage worms were treated for 36 h to avoid larval lethality.

Plasmids and generation of transgenes

To generate N-terminal RFP- and GFP-tagged transgenes for expression in the intestine of *C. elegans*, the skeleton vectors P*vha-6*::TagRFP-T and P*vha-6*::GFP were constructed by ligating the promoter region of *vha-6* followed by TagRFP-T and GFP sequences into Andrew Fire laboratory vector pPD49.26, respectively. The *wip-1* genomic DNA and *dbn-1* cDNA were digested with NcoI and XmaI, and individually cloned into the same sites of P*vha-6*::TagRFP-T-vector to generate N-terminal fusions. To construct P*vha-6*::TagRFP-T::RAB-5, the cDNA of *rab-5* was cloned into P*vha-6*::TagRFP-T-vector through the SmaI and KpnI sites. P*vha-6*::GFP::WIP-1 was constructed by ligating *wip-1* genomic DNA into P*vha-6*::GFP-vector at XmaI and KpnI sites. To generate the C-terminal RFP fusions P*vha-6*::DYN-1::TagRFP-T, P*vha-6*::ARX-2::TagRFP-T and P*vha-6*::CLIC-1::TagRFP-T, genomic fragments of *dyn-1* (digested by XmaI and KpnI) and *arx-2* (digested by XhoI and XmaI), and cDNA from *clic-1* (digested by XhoI and EcoRI) were individually inserted into the vector P*vha-6*::TagRFP-T, which was derived from Andrew Fire laboratory vector

Journal of Cell Science (2019) 132, jcs228023. doi:10.1242/jcs.228023

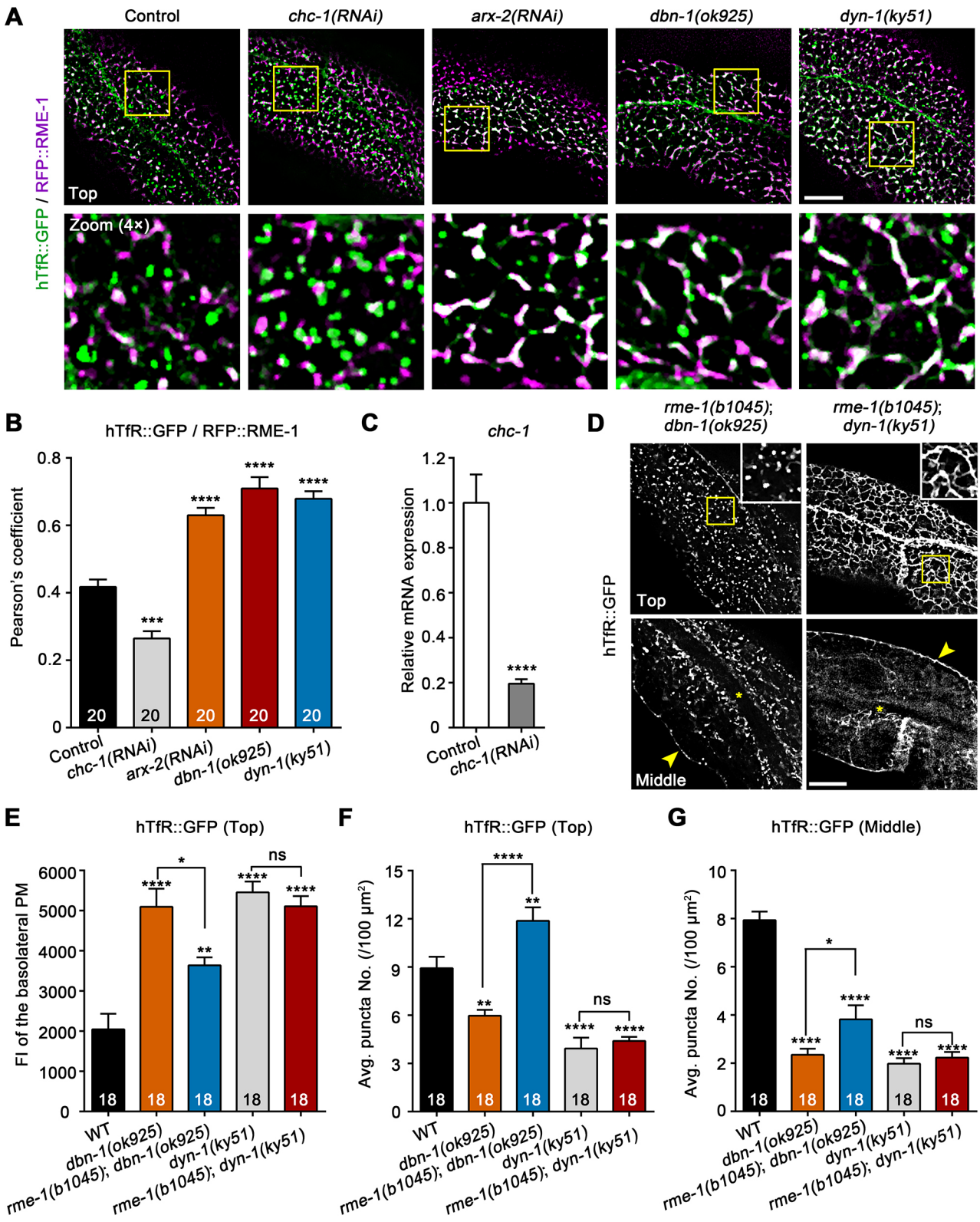

Fig. 5. See next page for legend.

pPD95.75. Lifeact::GFP reporter was made by inserting the 51-bp Lifeact fragment into pPD95.75-P*vha-6*::GFP through SmaI-AgeI sites. P*vha-6*::DYN-1::GFP and P*vha-6*::CLIC-1::GFP were constructed by replacing TagRFP-T with GFP. All of the deletion mutants for P*vha-6*::TagRFP-T::WIP-1, P*vha-6*::GFP::WIP-1 and P*vha-6*::TagRFP-T::DBN-1 were made by the overlap extension method (Horton et al., 1989). Standard microinjection methods were used to generate transgenic animals carrying extrachromosomal arrays. The standard injection mix consisted of 10 ng µl^{-1} plasmid, 10 ng µl^{-1} pRF4(*rol-6(su1006)*), as a co-injection marker, and 80 ng µl^{-1} PvuII-digested wild-type genomic DNA fragments.

Journal of Cell Science (2019) 132, jcs228023. doi:10.1242/jcs.228023

Fig. 5. Tubular endocytic intermediates caused by defective CCP scission are labeled and stabilized by RME-1. (A) Effects of *chc-1(RNAi)*, *arx-2(RNAi)*, *dbn-1(ok925)* or *dyn-1(ky51)* on RFP::RME-1 labeling of hTfR::GFP at the intestinal basolateral membrane. The lower panels are enlargements of the outlined areas. (B) Quantification of the Pearson's correlation coefficients to determine the level of colocalization for hTfR::GFP and RFP::RME-1 signals as depicted in A. (C) qRT-PCR analysis of the RNA silencing efficiency for *chc-1* gene. Data are mean±s.e.m. from three independent experiments. ****P<0.0001 (*t*-test). (D) Micrographs of hTfR::GFP-expressing intestines in *rme-1(b1045)*; *dbn-1(ok925)* or *rme-1(b1045)*; *dyn-1(ky51)* mutant animals at 25°C. Arrowheads indicate basolateral PM-associated hTfR::GFP. Asterisks depict the intestine lumen. The insets are magnified view of the boxed areas. (E–G) The average fluorescence intensity (FI) (E) and number of hTfR::GFP puncta (F) at the basolateral membrane and the number of hTfR::GFP puncta in the cytoplasm (G) were calculated for intestines of various genotypes as indicated. In B and E–G, the number of areas analyzed for each group is indicated in each bar. At least 18 animals were analyzed for each group. Data are mean±s.e.m. from three independent experiments. ns, not significant; *P<0.05; **P<0.01; ***P<0.001; ****P<0.0001 (one-way ANOVA). Top refers to the basolateral surface of the intestine, and Middle indicates a cross-section of the intestine. Scale bars: 10 µm.

Quantitative real-time PCR gene expression analysis

The total RNA of young adult worms was extracted with a MiniBEST Universal RNA Extraction Kit (TaKaRa) and a DNase I treatment step was performed to eliminate traces of genomic DNA. 1 µg total RNA was reverse transcribed to cDNA by using the RevertAid First Strand cDNA Synthesis Kit (Thermo Scientific) with oligo(dT) primers. All real-time PCR reactions were carried out by using the StepOne Plus Real-Time PCR System (Applied Biosystems) with SYBR Green real-time PCR master mix (TOYOBO). Relative expression was calculated by using a $2^{-\Delta\Delta Ct}$ method by normalizing to the expression of the tubulin α-2 chain (*tba-1*) housekeeping gene. Each experimental transcript was tested in quintuplicate. Samples without reverse transcriptase served as negative controls. Primers used are given in Table S2.

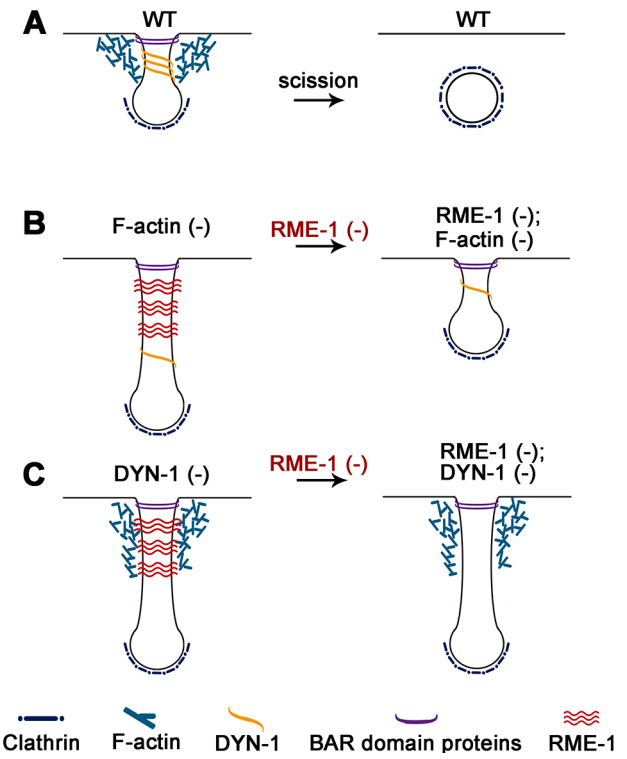

Fig. 6. Schematic representation of RME-1 participation in the arrested CCPs. (A) Proposed events for CCV generation in the wild-type: BAR proteins initiate membrane tubulation, and actin assembly provides the force against the plasma membrane and cooperates with DYN-1 for CCP scission. (B) Impairment of the actin assembly leads to overgrowth of the BAR-initiated tubules of endocytic intermediates because of RME-1 binding to the tubular templates and also attenuates the scission function of DYN-1. Simultaneous loss of RME-1 and F-actin results in formation of stalled CCPs and ceased endocytosis. (C) Scission defect arising from DYN-1 inactivation is not relieved by eliminating RME-1 due to F-actin assembly forcing the membranous tubules against the PM.

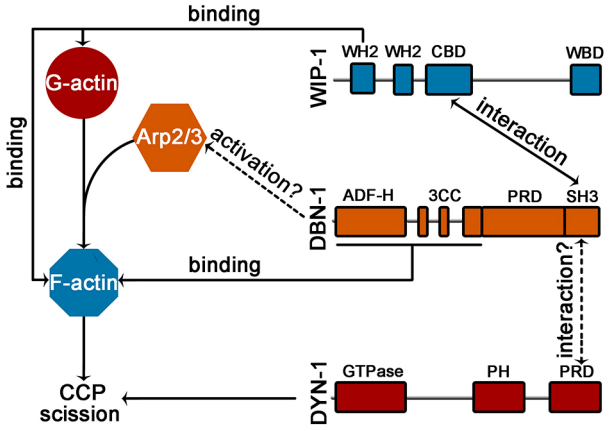

Fig. 7. Schematic representation of the interaction interfaces underlying F-actin and DYN-1 participation in CCP scission. WIP-1 binds to G-actin and F-actin through the first WH2 domain and contributes to DBN-1 recruitment to CCPs through a CBD–SH3 interaction. DBN-1 probably acts as a non-canonical NPF to activate Arp2/3-mediated actin assembly; it also binds to the assembled actin through its N-terminal ADF-H and 3CC domains, which is a prerequisite for DYN-1 recruitment to CCPs. In addition, DBN-1 may directly bind to DYN-1 through the SH3–PRD interaction.

Microinjection into the pseudocoelom

To disrupt actin polymerization in *C. elegans* intestine, 10 µM latrunculin B (Cayman Chemical) was injected into the pseudocoelom of young adult hermaphrodites 2 h before imaging. The drug was diluted in ethanol and used at a final concentration of 1% ethanol in egg buffer (118 mM NaCl, 48 mM KCl, 2 mM MgCl2, 2 mM CaCl2, and 25 mM Hepes pH 7.3). To examine the basolateral internalization of fluid-phase cargo, young adult hermaphrodites were microinjected with 0.5 mg ml^{-1} Rhod–Dex (10 kDa; Invitrogen) dissolved in egg buffer into the pseudocoelom at 1 h before imaging.

Confocal microscopy

Live young adult worms were mounted on a 2% (w/v) agarose pad with 10 mM levamisole (Sigma-Aldrich). Fluorescence images were obtained using a spinning-disc confocal system (CSU-X1 Nipkow; Yokogawa) equipped with an EM CCD camera (DU897K; ANDOR iXon) and oil-immersion objectives (60× N.A. 1.45 or 150× N.A. 1.45). Two 50 mW solidstate lasers (491 nm and 561 nm) coupled to an acoustic-optical tunable filter (AOTF) were used to excite GFP and RFP, respectively. The method to reduce interference from autofluorescence was previously described (Chen et al., 2014). *Z*-series of optical sections were acquired using a 0.3 µm step size. Time-lapse images were captured every 1.5 s (200 ms exposures) for 300 s.

Imaging analysis

Images were 3D deconvolved with three iterations by using AutoQuant X2 (Media Cybernetics) software. Brightness and contrast were adjusted for the images in ImageJ 1.52f (Wayne Rasband, National Institutes of Health). A 1.5-pixel-wide median filter and 10-pixel-wide rolling-ball background subtraction were used to increase the signal-to-noise ratio. To determine the average fluorescence intensity (FI) of basolateral PM-associated hTfR::GFP, a 10-pixel-wide region along basolateral PM was selected by using ImageJ 'Selection Brush Tool' and quantified. hTfR::GFP signals were pretreated with a wavelet transform algorithm and then analyzed with ImageJ 'Analyze Particles' for quantification of the puncta number and a customized Matlab

program for calculating the areas occupied by the signals (available from the corresponding author upon request), respectively. Tubular structures were identified by using ImageJ plugin 'Tubeness' and analyzed with the ImageJ plugin 'Skeleton'; the tubule length was calculated by a customized Matlab program (available from the corresponding author upon request). Kymographs were made by using AutoQuant. The time between the appearance of an object and its disappearance was calculated as lifetime, and lifetimes of the objects with fluorescent signal sustained during the span of the time-lapse series were treated as 300 s.

Colocalization analysis

The top layer stacks from two channels were imported to ImageJ for analysis. Pearson's coefficient was used for most cases, and was calculated by using the ImageJ plugin 'JACop'. The colocalization coefficients are expressed as percentage by scoring the RFP signals that are positive for GFP signals with respect to the total number of RFP puncta.

Statistical analysis

All data are presented as the mean±s.e.m. An unpaired two-tailed *t*-test was used to determine significant differences between two groups, and one-way ANOVA followed by a Tukey's *post hoc* test was used to evaluate differences between three or more groups. In case the sample did not assume normality, a Mann–Whitney rank test was performed. Statistical significance was as $P<0.05$ (*$P<0.05$; **$P<0.01$; ***$P<0.001$, ****$P<0.0001$; ns, not significant). All analyses were performed using Graphpad Prism 6 (GraphPad Software, La Jolla, CA). No inclusion or exclusion criteria were applied during analysis. The investigators were not blinded to allocation during experiments and outcome assessment. The worms were selected randomly within the same genotype.

Acknowledgements

We thank Professor Barth Grant (Rutgers University, Piscataway, NJ), the National BioResource Project (Tokyo Women's Medical University, Tokyo, Japan) and the *Caenorhabditis* Genetics Center (University of Minnesota, Minneapolis, MN) for providing *C. elegans* strains.

Competing interests

The authors declare no competing or financial interests.

Author contributions

Conceptualization: X.S., T.X., R.Z.; Methodology: X.S., F.D., T.X., R.Z.; Formal analysis: X.S., F.D., R.Z.; Investigation: X.S., F.D., L.L., Q.X.; Writing - original draft: X.S., L.L., T.X., R.Z.; Writing - review & editing: X.S., L.L., T.X., R.Z.; Funding acquisition: L.L., R.Z.

Funding

This work was supported by Grants from the National Natural Science Foundation of China (31571468; 31501119), the financial support of the Innovative Foundation of Huazhong University of Science and Technology (2016YXMS257) and the Major State Basic Research Program of China (2011CB910402).

Supplementary information

Supplementary information available online at
http://jcs.biologists.org/lookup/doi/10.1242/jcs.228023.supplemental

References

Anton, I. M. and Jones, G. E. (2006). WIP: a multifunctional protein involved in actin cytoskeleton regulation. *Eur. J. Cell Biol.* **85**, 295-304. doi:10.1016/j.ejcb.2005.08.004

Anton, I. M., Saville, S. P., Byrne, M. J., Curcio, C., Ramesh, N., Hartwig, J. H. and Geha, R. S. (2003). WIP participates in actin reorganization and ruffle formation induced by PDGF. *J. Cell Sci.* **116**, 2443-2451. doi:10.1242/jcs.00433

Bai, Z. (2015). A study of retrograde transport using *Caenorhabditis elegans* intestinal cells as a model. Dissertations & Theses - Gradworks. doi:10.7282/T3GQ70R6

Boulant, S., Kural, C., Zeeh, J.-C., Ubelmann, F. and Kirchhausen, T. (2011). Actin dynamics counteract membrane tension during clathrin-mediated endocytosis. *Nat. Cell Biol.* **13**, 1124-1131. doi:10.1038/ncb2307

Brenner, S. (1974). The genetics of *Caenorhabditis elegans*. *Genetics* **77**, 71-94.

Butkevich, E., Bodensiek, K., Fakhri, N., Von RODEN, K., Schaap, I. A. T., Majoul, I., Schmidt, C. F. and Klopfenstein, D. R. (2015). Drebrin-like protein DBN-1 is a sarcomere component that stabilizes actin filaments during muscle contraction. *Nat. Commun.* **6**, 7523. doi:10.1038/ncomms8523

Chen, C. C.-H., Schweinsberg, P. J., Vashist, S., Mareiniss, D. P., Lambie, E. J. and Grant, B. D. (2006). RAB-10 is required for endocytic recycling in the *Caenorhabditis elegans* intestine. *Mol. Biol. Cell* **17**, 1286-1297. doi:10.1091/mbc.e05-08-0787

Chen, S., Li, L., Li, J., Liu, B., Zhu, X., Zheng, L., Zhang, R. and Xu, T. (2014). SEC-10 and RAB-10 coordinate basolateral recycling of clathrin-independent cargo through endosomal tubules in *Caenorhabditis elegans*. *Proc. Natl. Acad. Sci. USA* **111**, 15432-15437. doi:10.1073/pnas.1408327111

Clark, S. G., Shurland, D.-L., Meyerowitz, E. M., Bargmann, C. I. and Van Der Bliek, A. M. (1997). A dynamin GTPase mutation causes a rapid and reversible temperature-inducible locomotion defect in *C. elegans*. *Proc. Natl. Acad. Sci. USA* **94**, 10438-10443. doi:10.1073/pnas.94.19.10438

Cortesio, C. L., Perrin, B. J., Bennin, D. A. and Huttenlocher, A. (2010). Actin-binding protein-1 interacts with WASp-interacting protein to regulate growth factor-induced dorsal ruffle formation. *Mol. Biol. Cell* **21**, 186-197. doi:10.1091/mbc.e09-02-0106

Da Costa, S. R., Sou, E., Xie, J., Yarber, F. A., Okamoto, C. T., Pidgeon, M., Kessels, M. M., Mircheff, A. K., Schechter, J. E., Qualmann, B. et al. (2003). Impairing actin filament or syndapin functions promotes accumulation of clathrin-coated vesicles at the apical plasma membrane of acinar epithelial cells. *Mol. Biol. Cell* **14**, 4397-4413. doi:10.1091/mbc.e03-05-0315

De La Fuente, M. A., Sasahara, Y., Calamito, M., Antón, I. M., Elkhal, A., Gallego, M. D., Suresh, K., Siminovitch, K., Ochs, H. D., Anderson, K. C. et al. (2007). WIP is a chaperone for Wiskott-Aldrich syndrome protein (WASP). *Proc. Natl. Acad. Sci. USA* **104**, 926-931. doi:10.1073/pnas.0610275104

Deo, R., Kushwah, M. S., Kamerkar, S. C., Kadam, N. Y., Dar, S., Babu, K., Srivastava, A. and Pucadyil, T. J. (2018). ATP-dependent membrane remodeling links EHD1 functions to endocytic recycling. *Nat. Commun.* **9**, 5187. doi:10.1038/s41467-018-07586-z

Engqvist-Goldstein, A. E. and Drubin, D. G. (2003). Actin assembly and endocytosis: from yeast to mammals. *Annu. Rev. Cell Dev. Biol.* **19**, 287-332. doi:10.1146/annurev.cellbio.19.111401.093127

Fares, H. and Greenwald, I. (2001). Genetic analysis of endocytosis in *Caenorhabditis elegans*: coelomocyte uptake defective mutants. *Genetics* **159**, 133-145.

Ferguson, S. M. and De Camilli, P. (2012). Dynamin, a membrane-remodelling GTPase. *Nat. Rev. Mol. Cell Biol.* **13**, 75-88. doi:10.1038/nrm3266

Ferguson, S. M., Raimondi, A., Paradise, S., Shen, H., Mesaki, K., Ferguson, A., Destaing, O., Ko, G., Takasaki, J., Cremona, O. et al. (2009). Coordinated actions of actin and BAR proteins upstream of dynamin at endocytic clathrin-coated pits. *Dev. Cell* **17**, 811-822. doi:10.1016/j.devcel.2009.11.005

Fried, S., Matalon, O., Noy, E. and Barda-Saad, M. (2014). WIP: more than a WASp-interacting protein. *J. Leukoc. Biol.* **96**, 713-727. doi:10.1189/jlb.2RU0314-162R

Gottlieb, T. A., Ivanov, I. E., Adesnik, M. and Sabatini, D. D. (1993). Actin microfilaments play a critical role in endocytosis at the apical but not the basolateral surface of polarized epithelial cells. *J. Cell Biol.* **120**, 695-710. doi:10.1083/jcb.120.3.695

Grant, B., Zhang, Y., Paupard, M. C., Lin, S. X., Hall, D. H. and Hirsh, D. (2001). Evidence that RME-1, a conserved *C. elegans* EH-domain protein, functions in endocytic recycling. *Nat. Cell Biol.* **3**, 573-579. doi:10.1038/35078549

Grassart, A., Cheng, A. T., Hong, S. H., Zhang, F., Zenzer, N., Feng, Y., Briner, D. M., Davis, G. D., Malkov, D. and Drubin, D. G. (2014). Actin and dynamin2 dynamics and interplay during clathrin-mediated endocytosis. *J. Cell Biol.* **205**, 721-735. doi:10.1083/jcb.201403041

Gryaznova, T., Kropyvko, S., Burdyniuk, M., Gubar, O., Kryklyva, V., Tsyba, L. and Rynditch, A. (2015). Intersectin adaptor proteins are associated with actin-regulating protein WIP in invadopodia. *Cell. Signal.* **27**, 1499-1508. doi:10.1016/j.cellsig.2015.03.006

Gryaznova, T., Gubar, O., Burdyniuk, M., Kropyvko, S. and Rynditch, A. (2018). WIP/ITSN1 complex is involved in cellular vesicle trafficking and formation of filopodia-like protrusions. *Gene* **674**, 49-56. doi:10.1016/j.gene.2018.06.078

Gu, C., Yaddanapudi, S., Weins, A., Osborn, T., Reiser, J., Pollak, M., Hartwig, J. and Sever, S. (2010). Direct dynamin-actin interactions regulate the actin cytoskeleton. *EMBO J.* **29**, 3593-3606. doi:10.1038/emboj.2010.249

He, K., Xing, R., Yan, X., Tian, A., Zhang, M., Yuan, J., Lv, Z., Fang, X., Li, Z. and Zhang, Y. (2015). Mammalian actin-binding protein 1/HIP-55 is essential for the scission of clathrin-coated pits by regulating dynamin-actin interaction. *FASEB J.* **29**, 2495-2503. doi:10.1096/fj.14-264259

Helgeson, L. A., Prendergast, J. G., Wagner, A. R., Rodnick-Smith, M. and Nolen, B. J. (2014). Interactions with actin monomers, actin filaments, and Arp2/3 complex define the roles of WASP family proteins and cortactin in coordinately regulating branched actin networks. *J. Biol. Chem.* **289**, 28856-28869. doi:10.1074/jbc.M114.587527

Horton, R. M., Hunt, H. D., Ho, S. N., Pullen, J. K. and Pease, L. R. (1989). Engineering hybrid genes without the use of restriction enzymes: gene splicing by overlap extension. *Gene* **77**, 61-68. doi:10.1016/0378-1119(89)90359-4

Hyman, T., Shmuel, M. and Altschuler, Y. (2006). Actin is required for endocytosis at the apical surface of Madin-Darby canine kidney cells where ARF6 and clathrin regulate the actin cytoskeleton. *Mol. Biol. Cell* **17**, 427-437. doi:10.1091/mbc.e05-05-0420

Itoh, T., Erdmann, K. S., Roux, A., Habermann, B., Werner, H. and De Camilli, P. (2005). Dynamin and the actin cytoskeleton cooperatively regulate plasma membrane invagination by BAR and F-BAR proteins. *Dev. Cell* **9**, 791-804. doi:10.1016/j.devcel.2005.11.005

Jackman, M. R., Shurety, W., Ellis, J. A. and Luzio, J. P. (1994). Inhibition of apical but not basolateral endocytosis of ricin and folate in Caco-2 cells by cytochalasin D. *J. Cell Sci.* **107**, 2547-2556.

Kamath, R. S., Martinez-Campos, M., Zipperlen, P., Fraser, A. G. and Ahringer, J. (2001). Effectiveness of specific RNA-mediated interference through ingested double-stranded RNA in *Caenorhabditis elegans*. *Genome Biol.* **2**, RESEARCH0002.

Kessels, M. M., Engqvist-Goldstein, A. E. and Drubin, D. G. (2000). Association of mouse actin-binding protein 1 (mAbp1/SH3P7), an Src kinase target, with dynamic regions of the cortical actin cytoskeleton in response to Rac1 activation. *Mol. Biol. Cell* **11**, 393-412. doi:10.1091/mbc.11.1.393

Kessels, M. M., Engqvist-Goldstein, A. E., Drubin, D. G. and Qualmann, B. (2001). Mammalian Abp1, a signal-responsive F-actin-binding protein, links the actin cytoskeleton to endocytosis via the GTPase dynamin. *J. Cell Biol.* **153**, 351-366. doi:10.1083/jcb.153.2.351

Kirchhausen, T. (2009). Imaging endocytic clathrin structures in living cells. *Trends Cell Biol.* **19**, 596-605. doi:10.1016/j.tcb.2009.09.002

Li, L., Wan, T., Wan, M., Liu, B., Cheng, R. and Zhang, R. (2015). The effect of the size of fluorescent dextran on its endocytic pathway. *Cell Biol. Int.* **39**, 531-539. doi:10.1002/cbin.10424

Martinez-Quiles, N., Rohatgi, R., Antón, I. M., Medina, M., Saville, S. P., Miki, H., Yamaguchi, H., Takenawa, T., Hartwig, J. H., Geha, R. S. et al. (2001). WIP regulates N-WASP-mediated actin polymerization and filopodium formation. *Nat. Cell Biol.* **3**, 484-491. doi:10.1038/35074551

Massaad, M. J., Oyoshi, M. K., Kane, J., Koduru, S., Alcaide, P., Nakamura, F., Ramesh, N., Luscinskas, F. W., Hartwig, J. and Geha, R. S. (2014). Binding of WIP to actin is essential for T cell actin cytoskeleton integrity and tissue homing. *Mol. Cell. Biol.* **34**, 4343-4354. doi:10.1128/MCB.00533-14

Mcghee, J. D. (2007). The *C. elegans* intestine (March 27, 2007), WormBook, ed. The C. elegans Research Community, WormBook. doi:10.1895/wormbook.1.133.1

Merrifield, C. J., Qualmann, B., Kessels, M. M. and Almers, W. (2004). Neural Wiskott Aldrich Syndrome Protein (N-WASP) and the Arp2/3 complex are recruited to sites of clathrin-mediated endocytosis in cultured fibroblasts. *Eur. J. Cell Biol.* **83**, 13-18. doi:10.1078/0171-9335-00356

Mise-Omata, S., Montagne, B., Deckert, M., Wienands, J. and Acuto, O. (2003). Mammalian actin binding protein 1 is essential for endocytosis but not lamellipodia formation: functional analysis by RNA interference. *Biochem. Biophys. Res. Commun.* **301**, 704-710. doi:10.1016/S0006-291X(02)02972-8

Mooren, O. L., Galletta, B. J. and Cooper, J. A. (2012). Roles for actin assembly in endocytosis. *Annu. Rev. Biochem.* **81**, 661-686. doi:10.1146/annurev-biochem-060910-094416

Pan, C. L., Baum, P. D., Gu, M., Jorgensen, E. M., Clark, S. G. and Garriga, G. (2008). *C. elegans* AP-2 and retromer control Wnt signaling by regulating mig-14/Wntless. *Dev. Cell* 14, 132-139. doi:10.1016/j.devcel.2007.12.001

Patel, F. B. and Soto, M. C. (2013). WAVE/SCAR promotes endocytosis and early endosome morphology in polarized *C. elegans* epithelia. *Dev. Biol.* **377**, 319-332. doi:10.1016/j.ydbio.2013.03.012

Qualmann, B. and Kessels, M. M. (2002). Endocytosis and the cytoskeleton. *Int. Rev. Cytol.* **220**, 93-144. doi:10.1016/S0074-7696(02)20004-2

Radhakrishna, H. and Donaldson, J. G. (1997). ADP-ribosylation factor 6 regulates a novel plasma membrane recycling pathway. *J. Cell Biol.* **139**, 49-61. doi:10.1083/jcb.139.1.49

Ramesh, N., Massaad, M. J., Kumar, L., Koduru, S., Sasahara, Y., Anton, I., Bhasin, M., Libermann, T. and Geha, R. (2014). Binding of the WASP/N-WASP-interacting protein WIP to actin regulates focal adhesion assembly and adhesion. *Mol. Cell. Biol.* **34**, 2600-2610. doi:10.1128/MCB.00017-14

Rodal, A. A., Sokolova, O., Robins, D. B., Daugherty, K. M., Hippenmeyer, S., Riezman, H., Grigorieff, N. and Goode, B. L. (2005). Conformational changes in the Arp2/3 complex leading to actin nucleation. *Nat. Struct. Mol. Biol.* **12**, 26-31. doi:10.1038/nsmb870

Sawa, M. and Takenawa, T. (2006). *Caenorhabditis elegans* WASP-interacting protein homologue WIP-1 is involved in morphogenesis through maintenance of WSP-1 protein levels. *Biochem. Biophys. Res. Commun.* 340, 709-717. doi:10.1016/j.bbrc.2005.12.056

Shi, A., Pant, S., Balklava, Z., Chen, C. C., Figueroa, V. and Grant, n (2007). A novel requirement for *C. elegans* Alix/ALX-1 in RME-1-mediated membrane transport. *Curr. Biol.* **17**, 1913-1924. doi:10.1016/j.cub.2007.10.045

Shi, A., Sun, L., Banerjee, R., Tobin, M., Zhang, Y. and Grant, B. D. (2009). Regulation of endosomal clathrin and retromer-mediated endosome to Golgi retrograde transport by the J-domain protein RME-8. *EMBO J.* **28**, 3290-3302. doi:10.1038/emboj.2009.272

Shi, A., Chen, C. C.-H., Banerjee, R., Glodowski, D., Audhya, A., Rongo, C. and Grant, B. D. (2010). EHBP-1 functions with RAB-10 during endocytic recycling in *Caenorhabditis elegans*. *Mol. Biol. Cell* **21**, 2930-2943. doi:10.1091/mbc.e10-02-0149

Sirotkin, V., Beltzner, C. C., Marchand, J.-B. and Pollard, T. D. (2005). Interactions of WASp, myosin-I, and verprolin with Arp2/3 complex during actin patch assembly in fission yeast. *J. Cell Biol.* **170**, 637-648. doi:10.1083/jcb.200502053

Spector, I., Shochet, N. R., Kashman, Y. and Groweiss, A. (1983). Latrunculins: novel marine toxins that disrupt microfilament organization in cultured cells. *Science* **219**, 493-495. doi:10.1126/science.6681676

Sun, Y., Martin, A. C. and Drubin, D. G. (2006). Endocytic internalization in budding yeast requires coordinated actin nucleation and myosin motor activity. *Dev. Cell* **11**, 33-46. doi:10.1016/j.devcel.2006.05.008

Taylor, M. J., Lampe, M. and Merrifield, C. J. (2012). A feedback loop between dynamin and actin recruitment during clathrin-mediated endocytosis. *PLoS Biol.* **10**, e1001302. doi:10.1371/journal.pbio.1001302

Timmons, L. and Fire, A. (1998). Specific interference by ingested dsRNA. *Nature* **395**, 854. doi:10.1038/27579

Welch, M. D. and Mullins, R. D. (2002). Cellular control of actin nucleation. *Annu. Rev. Cell Dev. Biol.* **18**, 247-288. doi:10.1146/annurev.cellbio.18.040202.112133

Zhu, X., Li, M., Xu, X., Zhang, R., Zhang, X., Ma, Z., Lu, J., Xu, T., Hou, J. and Song, E. (2018). hTAC internalizes via both clathrin-dependent and clathrin-independent endocytosis in mammalian cells. *Protein Cell* **9**, 896-901. doi:10.1007/s13238-018-0508-9

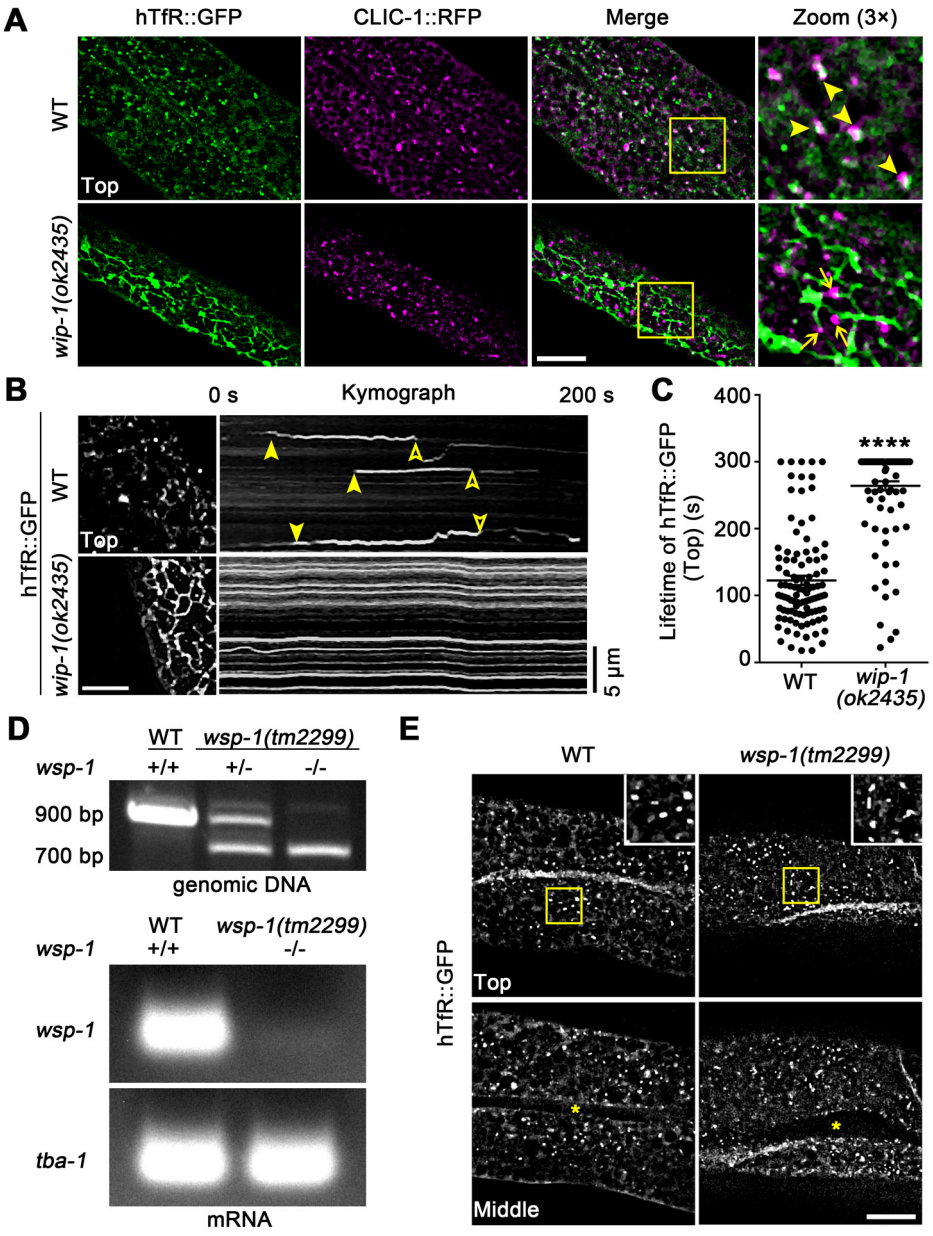

Fig. S1. WIP-1 function in CME in the *C. elegans* intestine is independent of WSP-1. (A) Colocalization images of hTfR::GFP with CLIC-1::RFP at the basal membrane in wild-type and *wip-1(ok2435)* mutant intestines. Insets show the enlargement of the indicated areas. Arrowheads point to positive overlap. Arrows indicate hTfR::GFP-tubules capped by CLIC-1::RFP upon loss of WIP-1. (B) Snapshots (Left) and kymographs (Right) of the representative time series from the basal membrane of the indicated intestines. Moments of hTfR::GFP appearance and disappearance are

marked by arrowheads. (C) Plots of individual lifetimes of hTfR::GFP from different intestines in wild-type and *wip-1(ok2435)* mutants, measured on dataset similar to B. *n*=100 events from 5 animals for each genotype. Data (mean±s.e.m.) were from three independent experiments in duplicate. ****P<0.0001 (Mann-Whitney). (D) PCR amplification of the targeted region using genomic DNA (Upper) or cDNA (Lower) extracted from each indicated genotype. (E) Representative confocal images show detailed distribution and architectures for intestinal hTfR::GFP signals in wild-type and *wsp-1(tm2299)* homozygotes. Asterisks depict the intestine lumen. Scale bars: 10 μm (A and E); 5 μm (B).

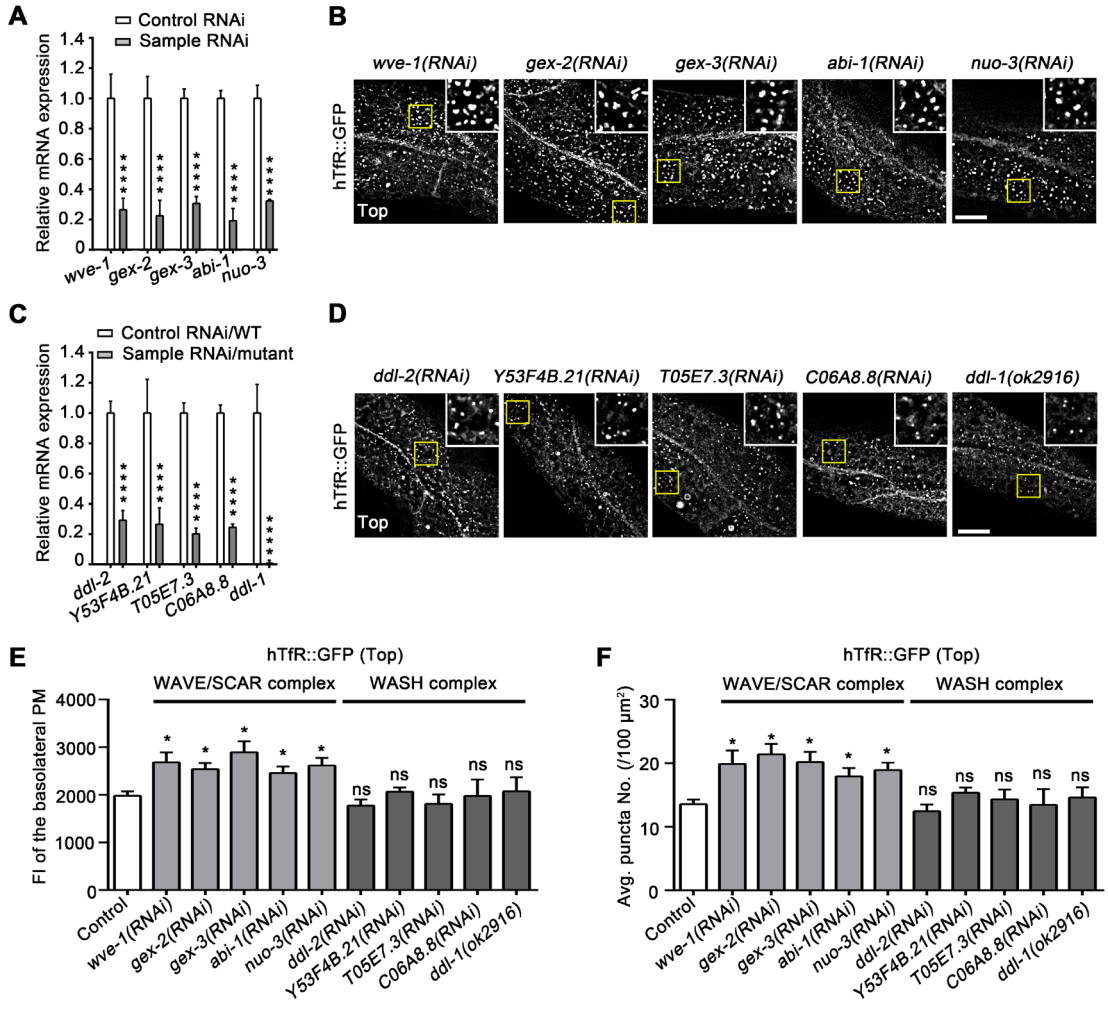

Fig. S2. Effect of disruption of WAVE/SCAR or WASH complex on the intestinal basal membrane-distributed hTfR::GFP. (A and C) qRT-PCR

quantification of the RNA silencing or knock-out efficiency for the individual WAVE/SCAR (A) or WASH (C) component genes. The mRNA levels in RNAi treatment animals were normalized to the levels in control animals, which were set as arbitrary unit 1. Data (mean±s.e.m.) were from three independent experiments. ****P<0.0001 (t-test). (B and D) Representative confocal images of hTfR::GFP at the intestinal basal membrane in worms depleting each component of the WAVE/SCAR (B) or WASH (D) complex. The insets are magnified view of the boxed areas. (E and F) Quantification of the average FI (E) and puncta number (F) of hTfR::GFP at the basal membrane depicted in B and D. n=20 regions from 20 animals were analyzed for each group. Data (mean±s.e.m.) were from three independent experiments. ns, not significant; *P<0.05 (one-way ANOVA). Scale bars: 10 µm.

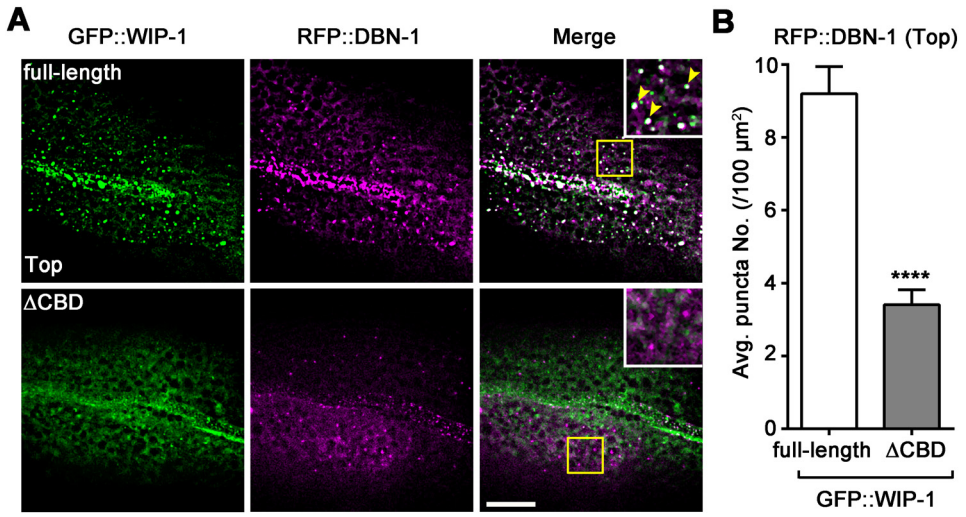

Fig. S3. CBD domain is essential for WIP-1 recruiting DBN-1 to CCPs. (A) Representative confocal images show the basal membrane localization of co-expressing GFP::WIP-1 full-length or ΔCBD construct with RFP::DBN-1. WIP-1 localization to the basal membrane was also influenced by the truncating deletion of CBD. Arrowheads indicate positive overlap. The insets are magnified view of the boxed areas. (B) The puncta number of RFP::DBN-1 per 100 µm^2 at the basal membrane were calculated for intestines depicted in A. n=20 regions from 20 animals were analyzed for

each group. Data (mean±s.e.m.) were from three independent experiments. ****P<0.0001 (Mann-Whitney). Scale bar: 10 µm.

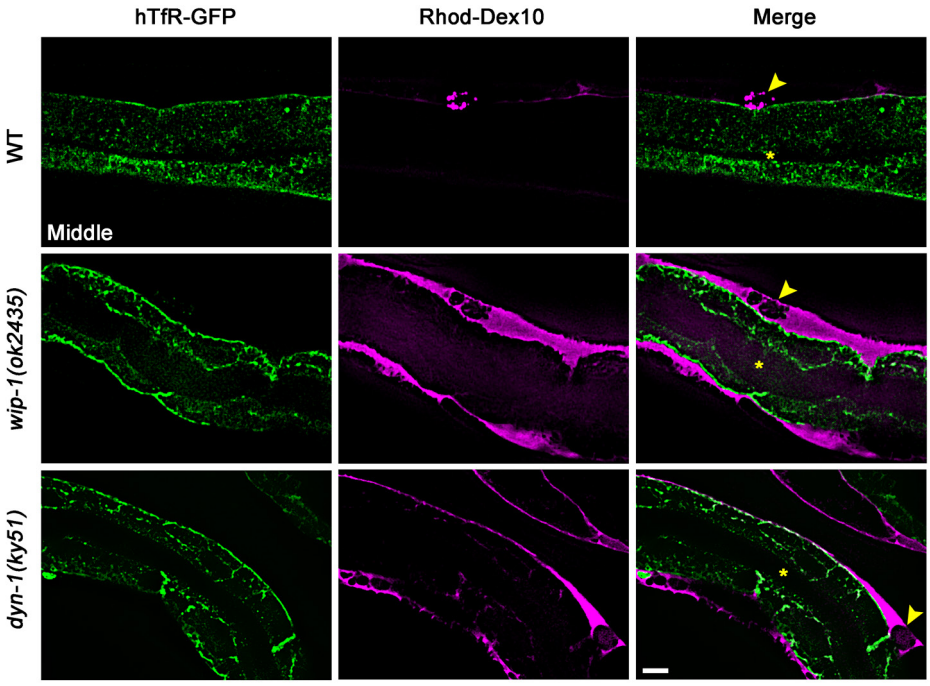

Fig. S4. Defective fluid-phase endocytosis of Rhod-Dex10 was induced in *wip-1(ok2435)* and *dyn-1(ky51)* mutants. Wild-type, *wip-1(ok2435)* and *dyn-1(ky51)* mutant intestines carrying hTfR::GFP exposed to basolateral Rhod-Dex10. Micrographs were taken 1 h after the Rhod-Dex10 injection into the pseudocoelom. The basolaterally internalized Rhod-Dex10 was fast-recycled out of the intestines back into the pseudocoelom and finally uptaken by the coelomocyte in wild-type animals, while in *wip-1(ok2435)* and *dyn-1(ky51)* mutant animals, Rhod-Dex10 was accumulated in the pseudocoeloms. Arrowheads point to coelomocytes, asterisks depict the lumen of the intestine. Scale bar: 10 µm.

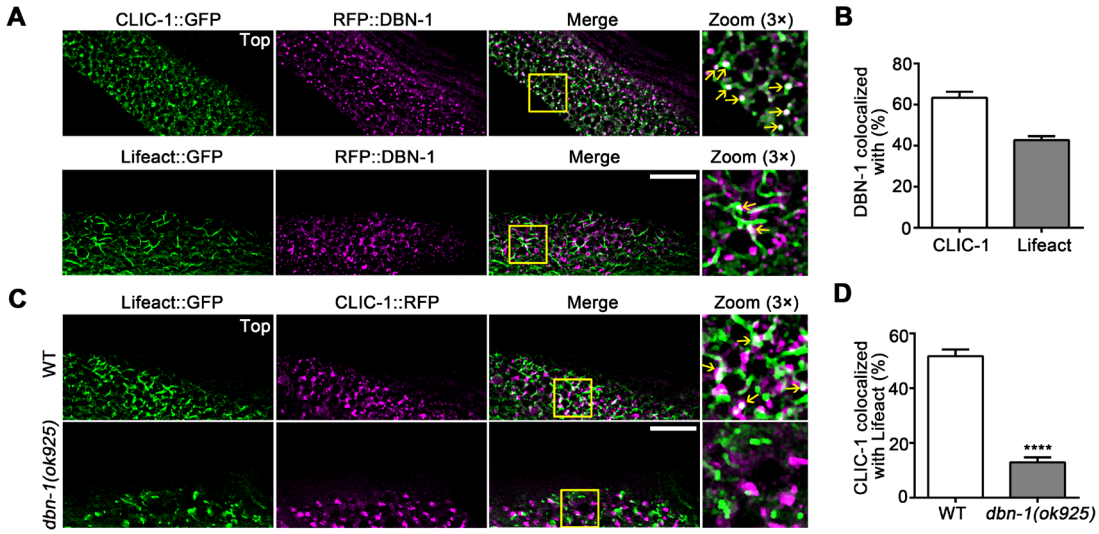

Fig. S5. DBN-1 promotes F-actin polymerization at the membrane-associated CCPs. (A and B) Representative colocalization images (A) and quantification (B) of RFP::DBN-1 with CLIC-1::GFP or Lifeact::GFP at the basal membrane. Insets show the enlargement of the indicated areas. Arrows indicate positive overlap. Note the decoration of DBN-1 on the tip or junction of Lifeact filaments. (C) Representative confocal images show the basal membrane localization of co-expressing Lifeact::GFP with CLIC-1::RFP in wild-type and *dbn-1(ok925)* mutants. Lifeact::GFP was obviously debranched and less colocalized with CLIC-1::RFP in *dbn-1* mutants. (D) Quantification of RFP-tagged CLIC-1 colocalized with Lifeact::GFP at the basal membrane for intestines of indicated genotypes. In B and D, *n*=15 regions from 12 animals for each group. Data (mean±s.e.m.) were from three independent experiments. ****P<0.0001 (Mann-Whitney). Scale bars: 10 µm.

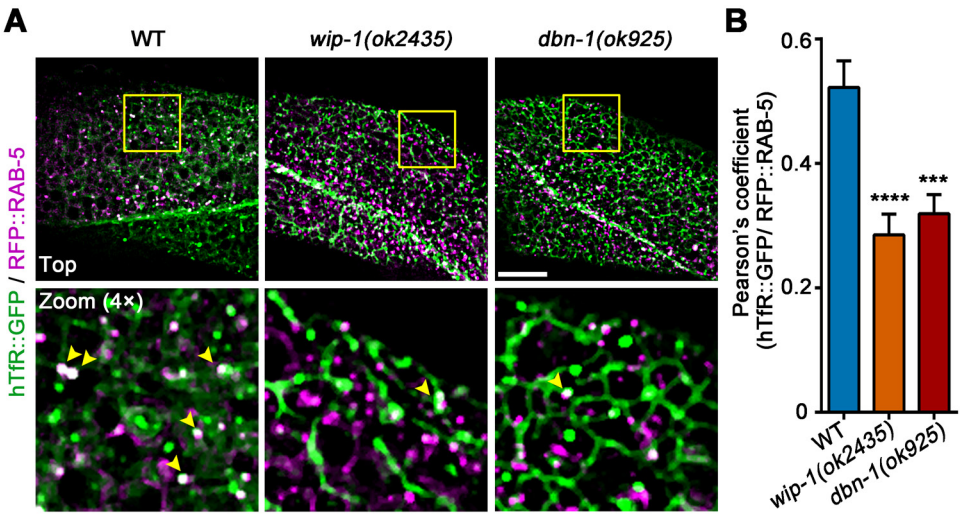

Fig. S6. The arrested hTfR-containing tubules caused by defective CCP scission are less labeled by RAB-5. (A) Colocalization images of hTfR::GFP with RFP::RAB-5 in wild-type, *wip-1(ok2435)* or *dbn-1(ok925)* mutant intestines. The Lower panels are enlargements of the outlined areas. Arrowheads indicate positive overlap. (B) Pearson's correlation coefficients for hTfR::GFP and RFP::RAB-5 signals depicted in A were calculated. *n*=20 regions from 20 animals for each genotype. Data (mean±s.e.m.) were from three independent experiments. ***P<0.001; ****P<0.0001 (one-way ANOVA). Scale bar: 10 µm.

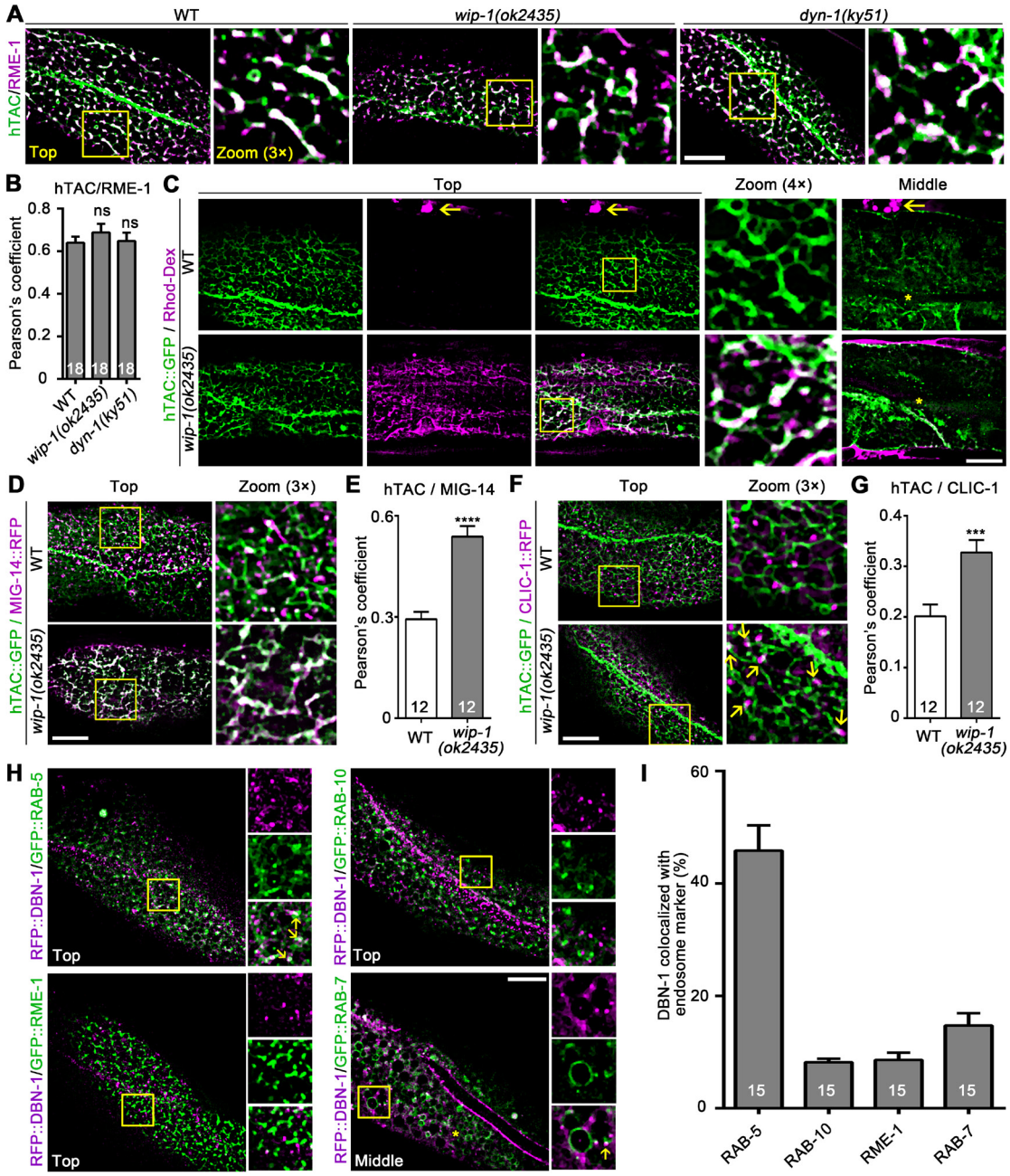

Fig. S7. WIP-1 also affects the internalization of hTAC in the intestine of *C. elegans*. (A) Colocalization images of hTAC::GFP with RFP::RME-1 in WT, *wip-1(ok2435)* and *dyn-1(ky51)* mutant intestines at 25°C. Insets are magnified view of the boxed areas. (B) Quantification of the colocalization by Pearson's colocalization coefficient. (C) Confocal images of basolaterally internalized Rhod-Dex10 in hTAC-GFP-expressing intestines of various mutants as indicated. Arrows indicate coelomocyte with internalized Rhod-Dex10. (D) Confocal images showing colocalization between

hTAC::GFP and MIG-14::RFP in the intestinal cells. hTAC tubules were extensively overlapped with the aberrant MIG-14 tubules in *wip-1* mutants. (E) Pearson's correlation coefficients for hTAC::GFP and MIG-14::RFP were calculated. (F) hTAC tubules were increasingly capped by clathrin in response to loss of WIP-1.(G) The levels of colocalization of hTAC::GFP and CLIC-1::RFP were determined by Pearson's correlation coefficients. (H and I) Representative colocalization images (H) and Quantification (I) of RFP::DBN-1 with GFP-tagged endosome markers in the intestine. Arrows indicate positive overlap. Asterisk depicts the intestine lumen. In B, E, G and I, the number of areas analyzed for each group is indicated in each bar. At least 12 animals were analyzed for each group. Data (mean±s.e.m.) were from three independent experiments. In B, ns, not significant (one-way ANOVA); In E and G, ****P<0.0001, ***P<0.001 (t-test). Scale bars: 10 μm.

Table S1. Mutant and transgenic strains used in this study.

Strain	**Genotype**
VC2053	*wip-1(ok2435) III* [a]
NG324	*wsp-1(gm324) IV* [a]
RB1004	*dbn-1(ok925) III* [a]
CX51	*dyn-1(ky51) X* [a]
VC2193	*ddl-1(ok2916) II* [a]
DH1201	*rme-1(b1045) V* [a]
tm2299	*wsp-1(tm2299) IV* [b]
RT1970	*unc-119(ed3) III; pwIs90[Pvha-6::hTfR::GFP, Cb-unc-119(+)]* [c]
RT2071	*unc-119(ed3) III; pwIs765[Pvha-6::MIG-14::GFP, Cb-unc-119(+)]* [c]
RT393	*unc-119(ed3) III; pwIs112[Pvha-6::hTAC::GFP, Cb-unc-119(+)]* [c]
RT548	*unc-119(ed3) III; pwIs216[Pvha-6::RFP::RME-1, Cb-unc-119(+)]* [c]
RT327	*unc-119(ed3) III; pwIs72[Pvha-6::GFP::RAB-5, Cbunc-119(+)]* [c]

RT525	*unc-119(ed3) III; pwIs206[Pvha-6::GFP::RAB-10, Cbunc-119(+)]* [c]
RT348	*unc-119(ed3) III; pwIs87[Pvha-6::GFP::RME-1, Cbunc-119(+)]* [c]
RT476	*unc-119(ed3) III; pwIs170[Pvha-6::GFP::RAB-7, Cbunc-119(+)]* [c]
RYZEx1	*[Pvha-6::TagRFP-T::WIP-1]* [d]
RYZEx2	*[Pvha-6::TagRFP-T::WIP-1(△1st WH2)]* [d]
RYZEx3	*[Pvha-6::TagRFP-T::WIP-1(△WBD)]* [d]
RYZEx4	*[Pvha-6::TagRFP-T::WIP-1(△CBD)]* [d]
RYZEx5	*[Pvha-6::GFP::WIP-1]* [d]
RYZEx6	*[Pvha-6::DYN-1::TagRFP-T]* [d]
RYZEx7	*[Pvha-6::DYN-1::GFP]* [d]
RYZEx8	*[Pvha-6::ARX-2::TagRFP-T]* [d]
RYZEx9	*[Pvha-6::TagRFP-T::DBN-1]* [d]
RYZEx10	*[Pvha-6::TagRFP-T::DBN-1(△ADF-H)]* [d]
RYZEx11	*[Pvha-6::TagRFP-T::DBN-1(△3CC)]* [d]
RYZEx12	*[Pvha-6::TagRFP-T::DBN-1(△PRD)]* [d]
RYZEx13	*[Pvha-6::TagRFP-T::DBN-1(△SH3)]* [d]
RYZEx14	*[Pvha-6::GFP::WIP-1(△CBD)]* [d]
RYZEx15	*[Pvha-6::CLIC-1::TagRFP-T]* [d]
RYZEx16	*[Pvha-6::CLIC-1::GFP]* [d]
RYZEx17	*[Pvha-6::Lifeact::GFP]* [d]
txuEx14	*[Pvha-6::TagRFP-T::RAB-5]* [d]

a. These mutant strains were provided by the *Caenorhabditis* Genetics Center (University of Minnesota, Minneapolis, MN). b. This strain was provided by the National BioResource Project (Tokyo Women's Medical University, Tokyo, Japan). c. These integrated transgenic strains were gifts from Professor Barth D. Grant (Rutgers University, Piscataway, NJ, USA). d. These extrachromosomal transgenic strains were obtained by using standard microinjection techniques.

Table S2. The specific primers used in Real-Time PCR analysis.

Gene	Primer	Oligo (5'-3')
wip-1	Forward	ACCATCCAGCAATGCTCGAAATG
	Reverse	CCATTTCCGTTTCCAGAATTTCC
wve-1	Forward	GCTTCAATGTACTGCTAATGGGAC
	Reverse	GTGATTTATTATCATTGCGTCGTG
gex-2	Forward	CTCTACAATGATGCTGCACAATACTCG
	Reverse	TCGAGAAGCATACACGACGCGAGCTG
gex-3	Forward	GTTAAAATTGGAGAAATGTCAGC
	Reverse	CAATTCGTGGAATACAGATAGCG
abi-1	Forward	GCGTAGCCTACCAGATTAACAAG
	Reverse	AATTTCTCGTCTTGCAAGCTTCTC
nuo-3	Forward	CCGCTTATAAGGAGTTCCAACG
	Reverse	TGAGTTTCTCCGACAAGTCTGTC
ddl-2	Forward	GAAGGGGAAATTCGATGGGATTC
	Reverse	CACTTTCCCATTGATCGCCTTCC
Y53F4B.21	Forward	GAAGGTCTACACCCGTATGCAACAG
	Reverse	GAAATAGCAGTAATTTGTCACG
T05E7.3	Forward	TGAAAGCTCTCTGAGTTGGAAAG
	Reverse	GTGCATTAGATATGTACTCAATC
C06A8.8	Forward	TCTCGTATGTCAGAGTTTAACAAC
	Reverse	CCCTTTCAGTGCATCTTCTCTTTC
ddl-1	Forward	TTTGATAAGAACCGTCGTAG
	Reverse	TGATGGAATCGAAATTGGCAGG
arx-2	Forward	TAAGGATTTGATGGTTGGCGAGG
	Reverse	TGCGCCATATCATCCCAGTTTC
chc-1	Forward	CAACGAGGCTTTGAATCAGTTGC
	Reverse	GCTTCCATCTGTTGTTTCCCTTG
wsp-1	Forward	TGGATCATGGTTCCGGAAAG

	Reverse	TATTCGAGAATCCACTATCC
tba-1	Forward	TGCTTGCTGGGAGCTCTACTGTCTC
	Reverse	CAACAACAGTTGGCTCAAGATCTAC